Enhancing superconductivity of $Lu_5Rh_6Sn_{18}$ by atomic disorder

A. Ślebarski,[1,2,*] M. Fijałkowski,[1] M. M. Maśka,[3] J. Deniszczyk,[4] P. Zajdel,[1] B. Trump,[5] and A. Yakovenko[6]

[1]*Institute of Physics, University of Silesia in Katowice, 75 Pułku Piechoty 1, 41-500 Chorzów, Poland*
[2]*Centre for Advanced Materials and Smart Structures, Polish Academy of Sciences, Okólna 2, 50-950 Wrocław, Poland*
[3]*Department of Theoretical Physics, Wroclaw University of Science and Technology, Wybrzeże Wyspiańskiego 27, 50-370 Wrocław, Poland*
[4]*Institute of Materials Engineering, University of Silesia in Katowice, 75 Pułku Piechoty 1A, 41-500 Chorzów, Poland*
[5]*Center for Neutron Research, National Institute of Standards and Technology, Gaithersburg, Maryland 20899, USA*
[6]*X-Ray Science Division, Advanced Photon Source, Argonne National Laboratory, Argonne, Illinois 60439, USA*

(Received 6 January 2021; revised 13 March 2021; accepted 25 March 2021; published 19 April 2021)

For a number of skutterudite-related cage compounds, such as cubic $R_3M_4Sn_{13}$ (R = Ca or La, M = transition d-electron metal) or tetragonal $Y_5Rh_6Sn_{18}$, we have previously reported the impact of various atomic defects in the crystal lattices on the normal-state and superconducting properties of these clathrates. In these quasiskutterudites the nanoscale disorder and/or local inhomogeneity in composition lead to an abnormal increase in the superconducting transition temperature T_c. Here we investigate the impact of atomic defects in the superconductors $Lu_{5-\delta}Rh_6Sn_{18}$ (tetragonal symmetry $I4_1/acd$). We have documented that $Lu_5Rh_6Sn_{18}$ does not crystallize in the assumed stoichiometry but forms a 5-6-18 phase with a Lu deficiency ($\delta \approx 0.5$). Our comprehensive investigations of electronic structure and thermodynamic and electrical transport properties documented a T_c increase in the more disordered sample (sample 1). The quality of two investigated samples (sample 1 and sample 2) with similar stoichiometry but different local inhomogeneity was obtained by microanalysis and electron transmission microscopy observations. The band structure calculations show a hybridization pseudogap in the electronic bands of stoichiometric $Lu_5Rh_6Sn_{18}$ at about 0.3 eV in respect to the Fermi level ϵ_F. The *ab initio* calculations predict the scenario that vacancies could shift this pseudogap towards ϵ_F, which is manifested by the Mott variable-range hopping behavior in the resistivity $\rho \sim T^{-1/4}$ of more homogeneous sample 2.

DOI: 10.1103/PhysRevB.103.155133

I. INTRODUCTION

The effect of disorder on superconductivity has been investigated on a variety of diverse superconducting materials for many decades. The earliest understanding of this phenomenon was due to Anderson's theorem [1] which predicts that the conventional BCS superconductors with isotropic superconducting s-wave gap generally are not sensitive to dilute nonmagnetic impurities, while even a small presence of magnetic dopants can drastically reduce the critical temperature of their superconducting state [2–4]. In the case of a strongly anisotropic gap, T_c should also be reduced by nonmagnetic impurities. Several theoretical calculations of T_c suppression have also discussed the pair-breaking effects of nonmagnetic scatterers on model multiband superconductors with generalized s-wave order [5]. This topic has received renewed attention because of several new reports of the observation of novel phenomena in a number of strongly disordered superconductors, especially at the limit of critical disorder leading to complete destruction of superconductivity [6,7]. In most investigated superconductors the disorder is associated with the presence of atomic scale disorder generated by impurities, structural defects, or local inhomogeneity, and it leads to electronic inhomogeneity over the length scales of the coherence length ξ. Therefore, unexpected observations of an enhancement of the superconducting transition temperature T_c, when the amount of disorder in a material is increased, are particularly interesting and have received our attention. In particular, the investigations of novel strongly correlated superconductors (SCS) [8–10] have shown that the atomic disorder, acting as a perturbation within the critical regime, can be decisive and changes the nature of the quantum macrostate either in the normal or superconducting phase. The disorder as perturbation can lead to novel phenomena like the disorder-enhanced superconductivity, discovered in a series of SCSs [10–16] and high-T_c $Bi_2Sr_2CaCu_2O_{8+x}$-type materials [17], however, the mechanism of T_c increasing is still under debate. Our present studies focus on the family of nonmagnetic skutterudite-related $R_3M_4Sn_{13}$-type superconductors (R = La, Y, or Ca, and M = d-electron-type metal) with the atomic scale disorder causing the appearance of a *novel high-temperature* superconducting state with the critical temperature $T_c^\star > T_c$ [15].

Several experimental and theoretical attempts have been undertaken to answer the question of why the superconductivity, characterized by the critical temperature T_c, is enhanced when the amount of disorder increases (e.g., Refs. [18,19]). Gastiasoro and Andersen [18] theoretically explained disorder-generated T_c increase for two separate scenarios: the dilute disorder case in multiband superconductors

*Author to whom correspondence should be addressed: andrzej.slebarski@us.edu.pl

 ©2021 American Physical Society

and dense disorder in conventional one-band superconducting systems. The proposed mechanisms model well enough the superconductivity of the disordered quasiskutterudites both at the small and large limit of disorder [19]. The current investigations of the series of $Lu_{5-\delta}Rh_6Sn_{18}$ quasiskutterudite compounds enable us to verify the validity of Gastiasoro and Andersen theoretical predictions for systems with low concentration of defects and those having strong fluctuation in homogeneity, as well as to predict experimentally the impact of the disorder strength on enhancement of the superconducting state.

II. EXPERIMENTAL AND COMPUTATIONAL DETAILS

The "$Lu_5Rh_6Sn_{18}$" (sample 1) and "$Lu_{4.6}Rh_6Sn_{18}$" (sample 2) polycrystalline samples were prepared by arc melting technique and then annealed at 870 °C for two weeks. All samples were examined by x-ray diffraction (XRD) analysis and found to have a tetragonal structure (space group $I4_1/acd$) [20,21]. Parametric XRD studies were carried out at the X-ray Science Division beamline 17BM [22] at the Advanced Photon Source, Argonne National Laboratory (Argonne, USA) with an incident x-ray energy of approximately 51 keV (wavelength $\lambda = 0.24177$ Å). Series of diffractograms were collected on a heat up ramp from 100 K to 500 K (360 K/h) using an area detector and processed using GSAS-II software package [23]. Structural serial refinements were carried out using FULLPROF software suite [24]. Temperature dependence of the cell volume was modeled using a second order Debye-Grüneisen fit described by Wood *et al.* [25]. The samples were labeled on the basis of the SEM study as $Lu_5Rh_6Sn_{18}$ (sample 1) and $Lu_{4.6}Rh_6Sn_{18}$ (sample 2), respectively. The naming scheme was preserved in the plots. Stoichiometry and homogeneity were checked by electron microprobe technique [scanning electron microscope JSM-5410 equipped with an energy-dispersive x-ray spectrometry (EDXS) microanalysis system]. The transmission electron microscopy (TEM) observations of the surface images and structural properties of nm size crystallites were performed using a JEOL high resolution (HRTEM) JEM 3010 microscope operating at a 300 kV accelerating voltage and equipped with a Gatan $2k \times 2k$ Orius™ 833SC200D CCD camera.

Electrical resistivity ρ was investigated by a conventional four-point ac technique using a PPMS (physical properties measurement system) device. Similarly, the PPMS platform was used to measure magnetic ac susceptibility. The dc magnetic susceptibility and magnetization measurements were carried out in the temperature range 1.8–400 K and in applied magnetic fields up to 7 T using a Quantum Design superconducting quantum interference device (SQUID) magnetometer.

The XPS spectra were obtained at room temperature in the vacuum of 8×10^{-8} Pa (6×10^{-10} Torr) using a PHI 5700 ESCA spectrometer with monochromatized Al K_α radiation. The samples were broken under a high vacuum before measuring the spectra.

The electronic band structure of stoichiometric $Lu_5Rh_6Sn_{18}$ was calculated using the full-potential linearized augmented plane waves (FP-LAPW) method complemented with local orbitals (LO) [26] implemented in the WIEN2K computer code [27]. The *ab initio* calculations were performed for the paramagnetic compound with the formula $Lu_{5-\delta}Rh_6Sn_{18}$, using the experimental lattice parameters (tetragonal structure, space group $I4_1/acd$) (for details on similarly made computations see, e.g., Ref. [28]). In the performed calculations we assumed the set of local orbitals (LO) and valence states (VB), respectively as follows: Lu—$[5s^25p^6]_{LO}\{4f^{14}5d^16s^2\}_{VB}$; Rh—$[4s^24p^6]_{LO}\{4d^85s^1\}_{VB}$; Sn—$[4p^64d^{10}]_{LO}\{5s^25p^2\}_{VB}$), and the scalar-relativistic Kohn-Sham was applied with spin-orbit coupling (SOC) accounted for by means of second variational method [26]. The gradient approximation form (GGA) of the exchange-correlation energy functional together with parametrization (PBEsol) derived for solids by Perdew *et al.* [29] were applied. The k mesh was tested against the total energy convergence and satisfactory precision, of few meV, was achieved with $7 \times 7 \times 7$ mesh [$N_k = 40\vec{k}$ vectors in irreducible Brillouin zone (*IBZ*)]. To account for the enhanced Coulomb correlation within $4f$ states of Lu and $4d$ states of Rh we applied the $LDA + U$ formalism [30].

III. RESULTS AND DISCUSSION

A. $Lu_{5-\delta}Rh_6Sn_{18}$: Microanalysis and structural properties

Our intention was to obtain the stoichiometric $Lu_5Rh_6Sn_{18}$ (labelled as sample 1) and off-stoichiometric $Lu_{4.6}Rh_6Sn_{18}$ (sample 2) compounds. It turns out, however, that system 5-6-18 does not crystallize in the assumed stoichiometry but forms a 5-6-18 phase with a Lu deficiency, and the obtained, arc-melted, $Lu_{5-\delta}Rh_6Sn_{18}$ compositions differ from the initially assumed stoichiometry (for both samples $\delta \approx 0.5$). The energy dispersive x-ray analysis gives the average Lu:Rh:Sn stoichiometric ratio for the sample surface, respectively, $4.55 \pm 0.25 : 6.0 \pm 0.23 : 17.75 \pm 0.30$ for sample 1 and $4.49 \pm 0.20 : 6.0 \pm 0.18 : 17.90 \pm 0.22$ for sample 2. Uncertainties are defined in the acknowledgments. For simplicity, the correct formulas of $Lu_{5-\delta}Rh_6Sn_{18}$-type compounds are replaced here by the expressions sample 1 and sample 2, respectively. EDXS indicates a similar atomic composition for sample 1 (initially assumed as $Lu_5Rh_6Sn_{18}$) and its Lu-deficient sample 2 variant. However, please note that the EDX picks up the signal from all phases present in the material and sample 1 will be shown to contain a tinlike impurity. In this sense, this is a phase content weighted average and might also include noncrystalline precipitations which are not picked up by the XRD. In sample 2, we do not see a clean signal from tin so it will be closer to the one phase system. This observation shows that the thermodynamic equilibrium in the Lu-rich melt is achieved by separation of tin and that a single phase system is achieved in a Lu deficient melt. A detailed structural characterization of the material is well beyond the size of this paper. The original paper of Hodeau *et al.* [21] on (Sn,Eu)-Rh-Sn single crystals serves as a good example for a complexity of such a task. The recent paper on a single crystal of "$Lu_5Rh_6Sn_{18}$" [31] (which was released after our submission) indicated that the Lu vacancy is filled by Sn. We have to note that the growth of a single crystal might have different thermodynamic equilibrium than arc melting and annealing of powder. Therefore, it does not have to give the same atomic

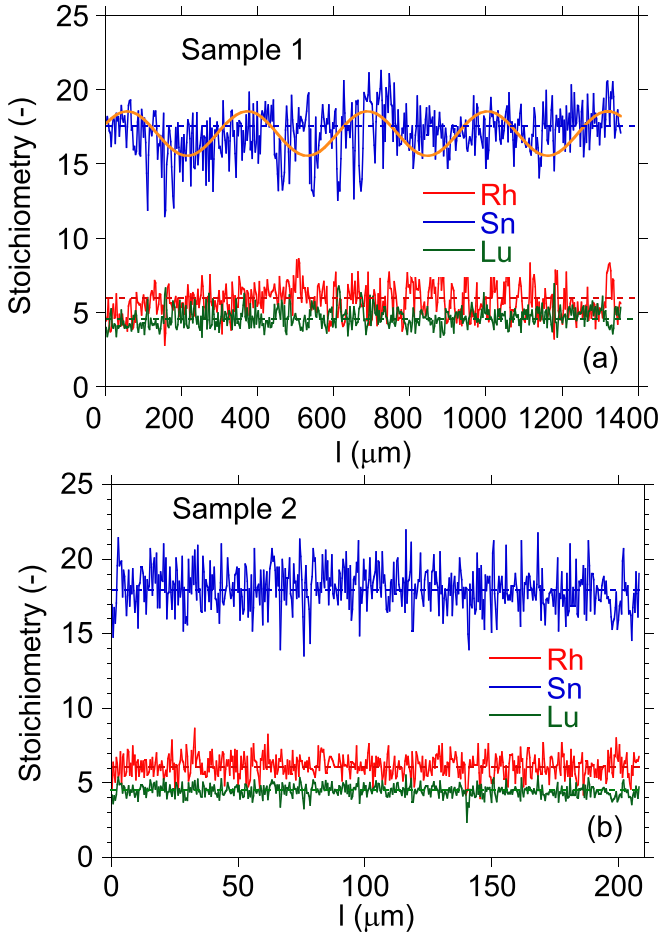

FIG. 1. Variation in stoichiometry of sample 1 [panel (a)] and sample 2 [panel (b)] over the length of the sample. The yellow curve in panel (a) is a rough approximation of the fluctuating Sn around mean content of 17.9 by $\Lambda \sin(\frac{2\pi}{\Delta l} l)$ function with amplitude $\Lambda = 1.6$ and $\Delta l = 23$ μm, where Δl could express a diameter of the extent of strong fluctuations in composition. $\Lambda \sin(\frac{2\pi}{\Delta l} l)$ function fits the experimental data in the region quite well up to about 800 μm, although the fluctuations in composition are observed for higher values of l too.

distribution as in our case. However, all studies show that the system is close to one phase equilibrium with a preference for deficiency of atoms in the Lu sites. Our recent TEM study on the (Y,Ca)-Rh-Sn system [19] has shown that even two separate but related structures like 3-4-13 ($Ca_3Rh_4Sn_{13}$) and 5-6-18 $(Y,Ca)_5Rh_6Sn_{18}$ can smoothly blend into each other within a few layers in one grain. We note that the 3-4-13 type cubic phase was not detected in this study, however, there are multiple structures related to the prototypical 3-4-13 system, for examples see Ref. [32]. Local fluctuations in stoichiometry over the length of the sample were observed at the nanoscale both in samples 1 and 2 due to intersite atomic disorder and/or atom displacements [33], as shown in Fig. 1. The stronger fluctuations in both atomic disorder and composition of larger volume fractions of ~20 μm are observed for sample 1, as panel (a) shows, while the effect is not visible for sample 2. We have recently shown [19] that similar fluctuations in concentration over larger areas of a sample volume of the isostructural compound $Y_5Rh_6Sn_{18}$ can significantly increase its superconducting temperature T_c, especially when the elemental local atomic disorder is strongly enhanced by doping. Likewise, we have expected that the local distortion in stoichiometry would also be the reason for a similar increase in T_c for sample 1. Indeed, within the investigated series of the $Lu_{5-\delta}Rh_6Sn_{18}$ compounds ($\delta \approx 0.5$), the superconducting transition temperature $T_c = 4.09$ K of sample 1 is evidently larger than $T_c = 3.69$ K of sample 2, for which the composition is more stable within the volume of the sample.

The structural studies revealed that sample 1 had a multiphase character with a minority phase initially identified as a tetragonal tin and another unidentified weak contribution. The tinlike impurity was not present in sample 2. The multiphase character of sample 1 indicates that its stoichiometry obtained by SEM is a sum of contributions from all of the phases present in the material. This problem was addressed in the XRD analysis, since it allows us to estimate the composition of each crystallographic phase separately. The structural models proposed here are based on the results of similar structural investigations for isostructural 5-6-18 crystals, previously reported by Hodeau *et al.* [21] and our group [28], and the notation for the formula unit was kept accordingly.

The large size of the tetragonal unit cell makes it impossible to uniquely refine all structural parameters even from a single crystal measurement. Therefore in this study, a simplified model based on our previous approach [19,28] was used. There were four main issues to be addressed during the refinement: (i) a mixed and possibly less than 1 occupancy of Lu1/Sn1 site, (ii) an incomplete occupancy of Lu2 site, (iii) fractional filling of the following Sn sites: Sn2, Sn31, Sn32, Sn33, Sn34, and Sn4, and (iv) large positional disorder vs "*rattling*" of the Sn4 site. Our previous results documented that the atomic displacement parameters (ADP) of the framework (Lu, Rh, Sn other than Sn4) are similar to each other ($\approx$1 Å^2) but differ significantly from the behavior of the Sn4 site (>3 Å^2), i.e., in the cage frame for the Sn4 site, its APD was at least five times larger than for the rest of the atoms. Therefore only two ADPs were used: the first one for the *rattling* Sn4 and the second one for all other atoms. Chemical occupancy of the sites was evaluated by refining different models from two datasets collected at 100 K and 500 K. No significant departures from a full occupancy were observed. Then, for the serial refinements, the number of parameters was further reduced by assigning full occupancy to all sites except the Lu1/Sn1 one, which might be prone to fractional occupancy [21]. The diffraction results confirm that fractional occupancy is not affected by the temperature. The XRD study allowed us to obtain structural information about the materials. For sample 1 an additional phase was identified as tetragonal tin with the mass fraction estimated to be 8.1(2)%. This phase was included in the refinement. We note, however, that a structural gray-tin-white-tin transition has not been observed down to 100 K, which means that the secondary phase is most probably the tin alloy [34]. An example of a complete set of patterns for sample 1 is presented in Fig. 2. The data presented in Table II were refined assuming first a full Lu1/Sn1 site occupancy with a refinable mixing factor. This approach was successful in the case of sample 1 (the first two columns) but resulted in negative Lu fraction for sample

TABLE I. Parameters obtained from a Grüneisen model of cell expansion [25]. N_{at}—number of atoms in the unit cell, θ_D—Debye temperature, V_0—cell volume at 0 K, $b = (K_0' - 1)/2$, $Q = V_0 K_0/\gamma_G$, where K_0 and K_0' are the incompressibility and its first derivative vs pressure, γ_G is a Grüneisen parameter. (*) Parameter b for sample 1 has *possibly* a nonphysical value which is connected with a non-Debye expansion (see Fig. 5).

Sample	N_{at}	θ_D (K)	V_0 (Å^3)	b (–)	Q (eV)
Sample 1	232	407(4)	5129.07(8)	−7.7(3)(*)	1466(7)
Sample 2	232	348(8)	5138.87(7)	3.7(3)	1921(9)
Sn	4	246(7)	107.722(6)	7.6(2)	18.8(2)

2 (the data are not presented in the table). Such behavior was indicative of a nonfull Lu1 site occupancy as was observed earlier by Hodeau *et al.* for $(Sn_{1-x}Er_x)Er_4Rh_6Sn_{18}$ [21] and our group for $(Sn_{1-x}Y_x)Y_4Rh_6Sn_{18}$ [28]. Despite this earlier observation we have tried to refine it anyhow, since the excess of tin in sample 1 suggested such a possibility. The final round of the refinements were performed for a fractional and only by Lu occupied the Lu1 sites (columns 3–6), in a way similar to previous studies. Modeling with the change of the Lu1 site occupation did not affect other structural parameters, which for the same conditions remained similar within a fitting error (columns 1 and 3, 2 and 4). The results indicate that both samples were affected by an off-stoichiometry obtained with large statistical uncertainties. This issue was encountered earlier in our previous studies of similar materials. A relative error of the occupancy of each tin site is less than 2.5%, but the number of Sn sites (up to 7) multiplies it to a significant value. Therefore, despite the fact that XRD does allow us to decouple compositions of each phase, the comparison and discussion with the SEM results from a large sample area is impossible (Fig. 3).

Comparison of the 100 K and 500 K datasets justifies the absence of significant relative atom movements within the cell. However, following our structural investigations of the inhomogeneity found in the system of $Y_{5-x}Ca_xRh_6Sn_{18}$ compounds, where two related structures of 3-4-13 and 5-6-18-type smoothly blend into each other within one grain [19], we have searched for similar subtle phase changes

TABLE II. Parameters of sample 1 and sample 2 superconductors obtained from the structural study. Space group $I4_1/acd$. For details of notation please check Ślebarski *et al.* [28]. $R_p/R_{wp}/R_{exp}$—conventional, background corrected, Rietveld factors. XRD composition is normalized to Rh_6, which for brevity is replaced with a (=).

Sample Model XRD compos.	Sample 1 (100 K) Sn1/Lu1 full $Lu_{3.7(3)}(=)Sn_{17(1)}$	Sample 1 (500 K) Sn1/Lu1 full $Lu_{3.7(2)}(=)Sn_{17(1)}$	Sample 1 (100 K) Lu1 fract. $Lu_{4.1(2)}(=)Sn_{17(1)}$	Sample 1 (500 K) Lu1 fract. $Lu_{4.1(2)}(=)Sn_{17(1)}$	Sample 2 (100 K) Lu1 fract. $Lu_{4.1(1)}(=)Sn_{16.9(8)}$	Sample 2 (500 K) Lu1 fract. $Lu_{4.2(1)}(=)Sn_{16.5(8)}$
a (Å)	13.7012(2)	13.7590(2)	13.7012(2)	13.7590(2)	13.7069(2)	13.7636(2)
c (Å)	27.3462(7)	27.4744(8)	27.3465(7)	27.4747(8)	27.3735(5)	27.4837(6)
V (Å^3)	5133.5(2)	5201.2(2)	5133.6(2)	5201.2(2)	5142.9(1)	5206.4(2)
B_{iso} other (Å^2)	0.48(4)	1.39(4)	0.51(4)	1.42(4)	0.44(3)	1.17(3)
B_{iso} Sn4 (Å^2)	5.9(4)	7.0(3)	5.7(4)	6.9(3)	3.1(2)	4.0(2)
SOF Lu1/Sn1	0.40/0.60(2)	0.40/0.60(2)	0.796(4)/0	0.800(4)/0	0.580(4)/0	0.572(4)/0
z_{Rh1}	−0.0032(7)	−0.0034(8)	−0.0030(7)	−0.0032(8)	−0.0036(6)	−0.0034(6)
x_{Rh2}	0.2421(6)	0.2424(8)	0.2422(6)	0.2424(8)	0.2437(6)	0.2438(6)
y_{Rh2}	0.2486(5)	0.2490(5)	0.2487(5)	0.2491(5)	0.2504(4)	0.2502(4)
z_{Rh2}	−0.125(2)	−0.125(2)	−0.125(2)	−0.125(2)	−0.1249(7)	−0.1252(7)
x_{Lu2}	0.1327(5)	0.1320(5)	0.1327(5)	0.1320(5)	0.1328(3)	0.1319(4)
y_{Lu2}	0.3864(5)	0.3853(5)	0.3864(5)	0.3853(5)	0.3867(3)	0.3862(3)
z_{Lu2}	−0.1920(2)	−0.1920(2)	−0.1920(2)	−0.1920(2)	−0.1926(2)	−0.19220(2)
x_{Sn2}	0.0884(6)	0.0894(6)	0.0887(6)	0.0895(6)	0.0874(4)	0.0888(5)
y_{Sn2}	0.3380(6)	0.3394(5)	0.3380(6)	0.3394(6)	0.3385(4)	0.3393(4)
z_{Sn2}	−0.0787(3)	−0.0782(3)	−0.0789(3)	−0.0783(3)	−0.0806(2)	−0.0806(2)
x_{Sn31}	0.1811(5)	0.1786(6)	0.1815(6)	0.1790(6)	0.1746(6)	0.1727(5)
x_{Sn32}	0.3193(6)	0.3216(7)	0.3188(6)	0.3212 (7)	0.3276(6)	0.3291(5)
x_{Sn33}	0.3300(10)	0.3289(11)	0.3301(10)	0.330(2)	0.3262(6)	0.3256(6)
y_{Sn33}	0.2619(5)	0.2615(5)	0.2619(5)	0.2613(5)	0.2622(4)	0.2620(4)
z_{Sn33}	−0.0383(6)	−0.0381(7)	−0.0384(6)	−0.0382(7)	−0.0389(3)	−0.0392(3)
x_{Sn34}	0.0070(5)	0.0046(5)	0.0069(5)	0.0045(5)	0.0040(3)	0.0025(4)
y_{Sn34}	0.5773(10)	0.5769(12)	0.5778(10)	0.5775(12)	0.5710(8)	0.5687(7)
z_{Sn34}	−0.0377(6)	−0.0378(8)	−0.0377(6)	−0.0378(8)	−0.0364(4)	−0.0358(4)
y_{Sn4}	0.4692(8)	0.4732(8)	0.4692(8)	0.4732(8)	0.4614(4)	0.4621(5)
$R_p/R_{wp}/R_{exp}$	10.9/12.8/3.01	11.0/12.0/3.46	11.0/12.8/3.01	11.0/12.1/3.46	7.43/9.64/3.22	8.32/10.4/3.51

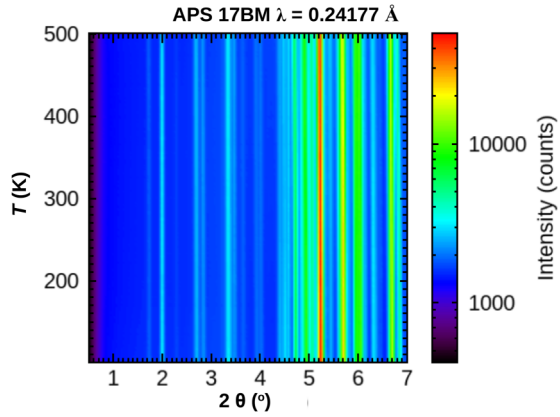

FIG. 2. Low angle section of the merged diffractograms for sample 1. Intensity is presented on a logarithmic scale to magnify weak peaks.

in $Lu_{5-\delta}Rh_6Sn_{18}$. For this purpose, the full temperature range was fit using a second order Debye-Grüneisen model for the cell expansion with parametrization suggested by Wood

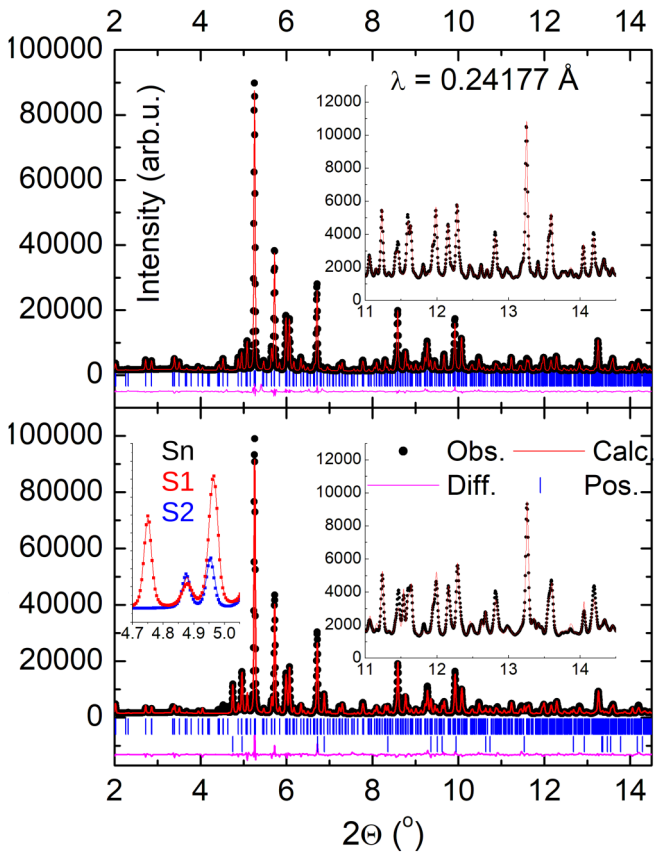

FIG. 3. Plots of Rietveld refinement for sample 2 (top) and sample 1 (bottom). Black dots—observed pattern, red line—calculated, blue ticks—Bragg peak positions, magenta line—the difference. Insets in each plot show magnified regions from the end of the patterns. On the bottom plot, the second set of blue markers indicates positions of tin impurity, which is enhanced in the inset "Sn" in the bottom panel. The two strongest reflections visible in the bottom panel from the tinlike phase in sample 1 (red line) are (200) at 4.75 deg and (101) at 4.97 deg, respectively. They are not present in sample 2 (blue line).

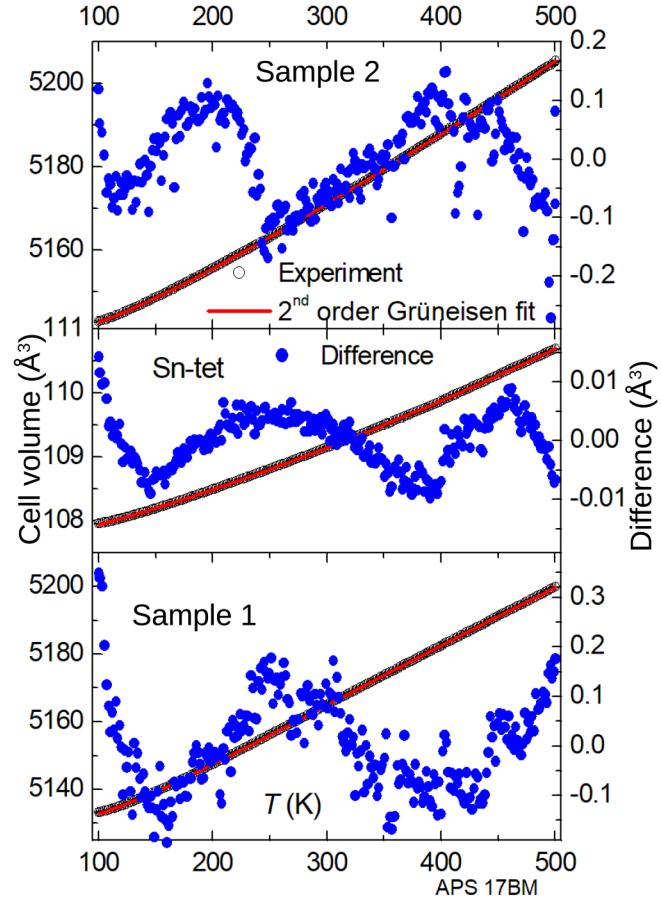

FIG. 4. Temperature dependence of cell volumes for the refined phases (black circles) were fit with a second-order Grüneisen fit (red line). The error bars of the refined parameters are smaller than the circle size (0.19 Å^3 for Lu phases and 0.007 Å^3 for the tinlike impurity). The left axis presents differences between the experiment and the fit (blue dots).

et al. [25]. The results of this approach for both 5-6-18 phases and the tin impurity are presented in Fig. 4 and in Table I. The fitting gave very good results in the case of sample 1 and the tinlike impurity. For Sn-rich impurity phase the obtained Debye temperature agrees well with the tabulated value [35]. For sample 2 the obtained θ_D value is higher than that expected from other measurements. One notes, however, that the strong enhancement of the highest phonon frequency $\omega_D \sim 1/M^{1/2}$ is expected due to the presence of rhodium, which is lighter than tin. Additionally, this value of θ_D might be different from that obtained from the low temperature specific heat data, as different and much higher phonon modes might be available at high temperatures. The problem in determination of θ_D arises for sample 1, for which we have obtained a negative value of parameter b that we obtained (b describes dependence of incompressibility on pressure, see Table I). This behavior most likely indicates a phase transition (or an additional effect) disturbing the fit. In order to inspect this fact without imposing any physical model, we followed a procedure applied earlier [28], which was based on a simple linear fit to volume change $V(T)$ in the temperature region between 150 K and 450 K, with accompanying T

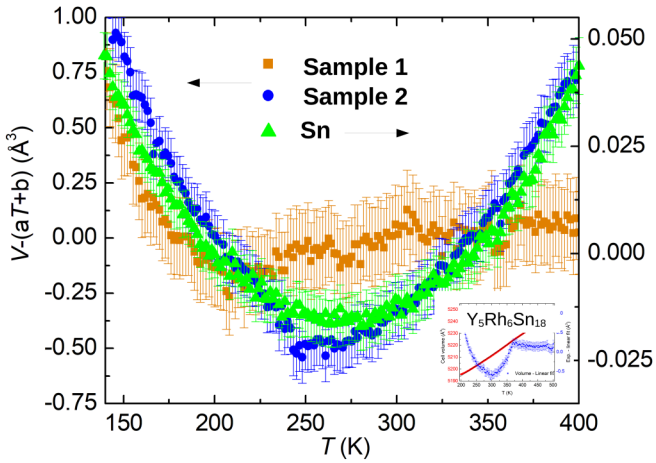

FIG. 5. Differences in the unit cell volume expansion visualized by a simple linear fit from 150 K to 400 K reveal similar behavior for sample 2 (blue) and the tinlike impurity (green). Sample 1 (brown) displays a trend similar to $Y_5Rh_6Sn_{18}$ [28] which is included as an inset in the right bottom corner. Sample 1 might not follow a Grüneisen-like evolution. Error bars represent 1-σ confidence level.

anomalies in resistivity and specific heat (see Sec. III C). The differences $\Delta V = V - (aT + b)$ for all materials are presented in Fig. 5. The change $\Delta V(T)$ is similar for sample 2 and the impurity Sn-based phase, while it looks different for sample 1. This behavior could only suggest a possible phase transition in sample 1, however, this behavior is not an unequivocal confirmation of the structural transition. The $\Delta V(T)$ looks similar to the one presented for the $Y_5Rh_6Sn_{18}$ [28] (Fig. 13 therein).

B. Band structure of $Lu_5Rh_6Sn_{18}$, electrical resistivity, and thermodynamic characterization

The *ab initio* calculations documented that the correlation energy U significantly modifies the calculated Lu $4f$ electronic states of stoichiometric $Lu_5Rh_6Sn_{18}$ within the range of binding energies ($-12 < E < -6$) eV, while its impact on the shape of the total density of states (TDOS) located between -6 eV and the Fermi energy is negligible. For DFT calculations we have chosen an effective Coulomb correlation parameter $U_f = (3, 4.5, 5.5,$ and $6.8)$ eV. For all calculations made for a number of different ($0 \leqslant U_f \leqslant 6.8$) eV, the d-electron correlations with $U_d = 3$ eV were always taken into account the same [36,37]. Figure 6 compares the valence XPS spectra of sample 1 and sample 2 with the calculated TDOS for $U_f = 3$ eV (blue line) and 6.8 eV (brown line), respectively. The Lu $4f$-electron XPS states are well accounted for by the Lu $4f$ states calculated for $U_f = 6.8$ eV, which suggests that the DFT calculations with $U_f = 6.8$ eV and accompanying $U_d = 3$ eV are the most reasonable for obtaining the details in the electronic bands near the Fermi level and the value of TDOS, $2N(\epsilon_F)$, at ϵ_F. Figure 7 shows the energy distribution of the summarized s, p, d, and f electronic states for all Lu, Rh, and Sn atoms in the $Lu_5Rh_6Sn_{18}$ formula unit, located in the bands near the Fermi level. Thus, it is possible to precisely determine the contributions of various conduction electrons to the electrical transport of $Lu_5Rh_6Sn_{18}$, as well as

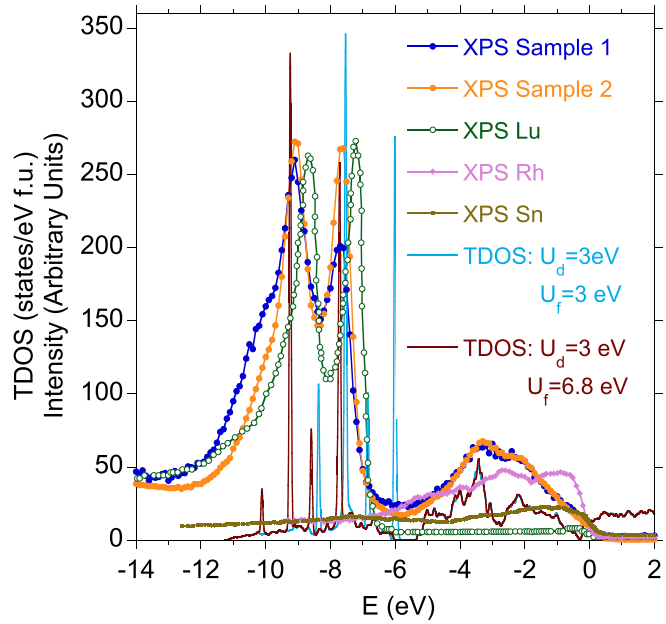

FIG. 6. Valence band XPS spectra for sample 1 (blue points) and sample 2 (orange points) are compared with the calculated total DOS within the LSDA approximation. The blue curve shows the TDOS calculated for $U_f = 3$ eV and $U_d = 3$ eV, while the brown curve shows the calculated TDOS with $U_f = 6.8$ eV and $U_d = 3$ eV. The VB XPS spectra, measured for pure Lu, Rh, and Sn metals, are also shown. The intensities of all measured VB XPS bands are renormalized to the background for sample 1 at $E > \epsilon_F$.

explain the different $\rho(T)$ characteristics obtained for sample 1 and more off-stoichiometric sample 2.

The VB XPS spectra shown in Fig. 6 are dominated either by the Rh $4d$ and Sn $5p$ states near ϵ_F or by Lu $4f$ states located deeply between -6 eV and -11 eV in the valence XPS bands. For binding energies (-3 to -11) eV the Sn $5s$ states also give a significant contribution to the intensity of the VB XPS spectra. We also studied the binding energy spectrum of individual atoms to provide information about the ionic state of atoms and thus the change in local structure and better information about disorder within the unit cell and disorder in composition. To make a comparison, we measured the XPS spectra of Sn, Rh, and Lu metals. Figure 6 shows the VB XPS spectra for the reference metals, where all spectra displayed in the figure are normalized to the background intensity for sample 1. The Sn $5p$ XPS states measured for metallic tin show two broad maxima at the binding energy of $\sim$1.3 eV and $\sim$7.3 eV, while both the maxima are not present in the VB XPS spectra for sample 1 and 2, because they are covered by the Rh $4d$ and Lu $4f$ states, respectively. Therefore the analysis of the relative energy shift of the Sn $5p$ states located in the VB XPS spectra shown in Fig. 6 in respect to Sn metal is impossible. The VB XPS spectrum for pure Rh metal shows two maxima, at 2.1 eV and 2.8 eV, addressed to the distribution of the $4d$ electron states. Both maxima are also observed in the VB XPS spectra of sample 1 and 2 at about 2.3 and 3.3 eV. We suggest that the charge redistribution, due to covalent bonding between Rh and Lu states [38], is the dominating effect on the atomic $4d$-level

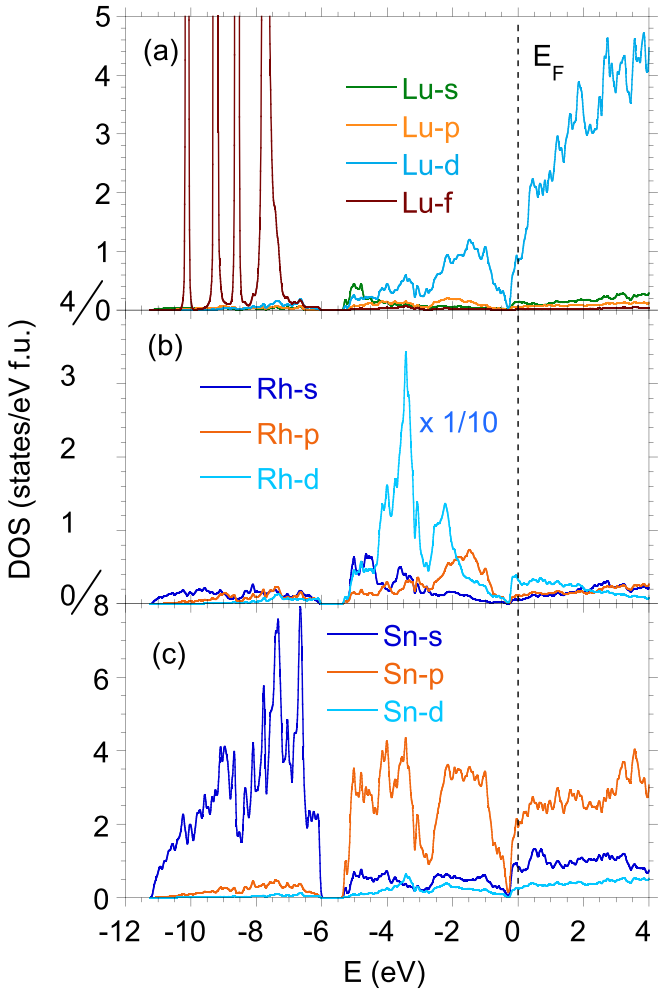

FIG. 7. Sum of the s, p, and d electronic states in respective valence bands of Lu, Rh, and Sn in the $Lu_5Rh_6Sn_{18}$ formula unit, distributed near the Fermi level. All partial DOSs are calculated for $U_f = 6.8$ eV and $U_d = 3$ eV. In panel (b) total density of d-electron states calculated for four Rh atoms is multiplied by $1/10$ to present all remaining atomic DOSs with the same scale.

shift, very similar in both samples. Perhaps most interesting is the information about the ionic state of Lu atoms and thus the change in local structure, as shown in Fig. 6. For this purpose, the $4f$ spectra of metallic Lu were compared with the $4f^{5/2}$ and $4f^{7/2}$ states in VB XPS spectra of the $Lu_5Rh_6Sn_{18}$ sample and its off-stoichiometric variant. For Lu metal the maxima of $4f^{5/2}$ and $4f^{7/2}$ XPS lines are at binding energy of 7.3 eV and 8.7 eV, respectively. While these maxima are clearly detected in the related VB XPS bands of sample 1 and sample 2, they are shifted to higher binding energies 7.7 eV and 9.1 eV, respectively. Again, from a similar atomic $4d$-level shift one can speculate the formation of covalent bondings between Lu and neighboring atoms for both samples, however, one cannot discuss strength of local disorder. However, the broader distribution of the $4f$ states documented for sample 1 gives arguments for stronger disorder, both compositional and within the unit cell, compared to sample 2.

It is worth noting that at the binding energy around $E = -0.3$ eV there is a hybridization pseudogap in TDOS (see

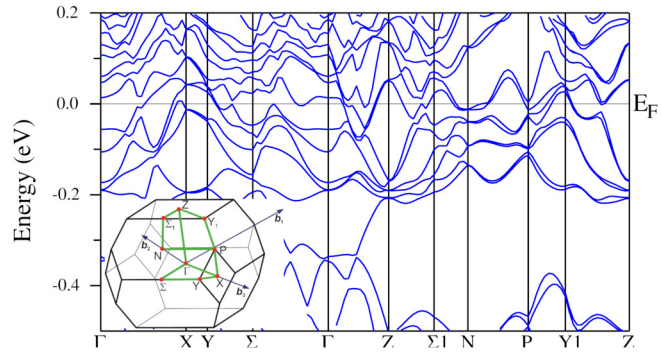

FIG. 8. The band structure calculated along high symmetry k lines in the Brillouin zone (shown in the inset) of $Lu_5Rh_6Sn_{18}$ for $U_f = 6.8$ eV and accompanying $U_d = 3$ eV.

also Fig. 8), which can be shifted towards the Fermi level by the structural defects, as was documented by our previous *ab initio* calculations carried out for similar quasiskutterudites [38,39]. It will be discussed below. The bands of

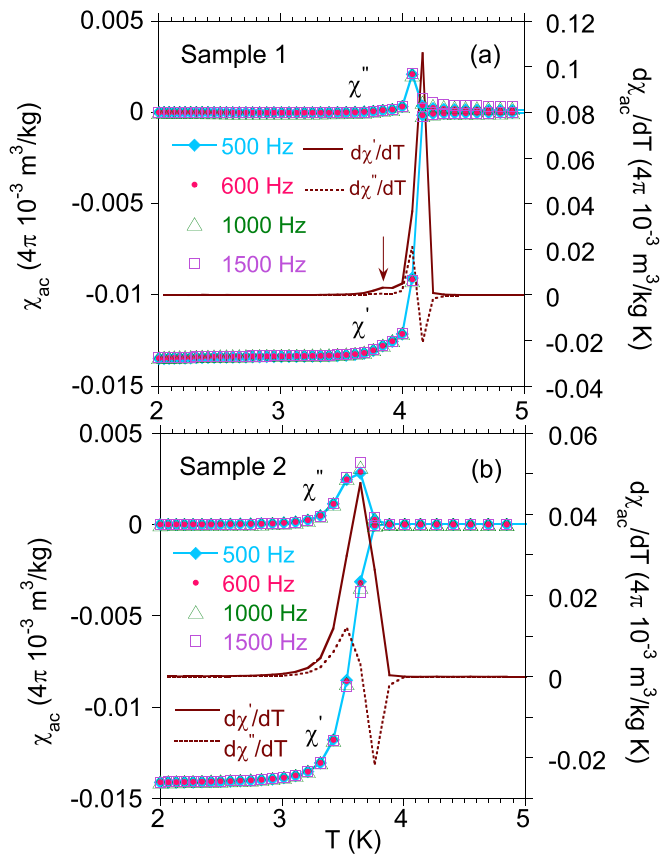

FIG. 9. Temperature dependencies of the real χ' and imaginary χ'' components of the ac mass magnetic susceptibility χ_{ac} per 1 Oe for sample 1 [panel (a)] and sample 2 (b), measured at different frequencies ν, and derivative $d\chi'/dT$ and $d\chi''/dT$ [the used unit $4\pi \times 10^{-3}$ m^3/kg (SI) is equivalent to 1 emu/g (cgs)]. Panel (a) displays the data for inhomogeneous sample 1, the first maximum in $d\chi'/dT$ is assigned to $T_c^\star$ of the inhomogeneous phase, the second weak maximum at ~3.85 K marked by an arrow is referred to the formation of the bulk T_c phase. Panel (b) shows a broad transition to the superconducting state of sample 2 with very similar T_c and $T_c^\star$.

TABLE III. Superconducting and normal state (n) quantities for $Lu_{5-\delta}Rh_6Sn_{18}$ (sample 1 and sample 2): normal state electronic specific heat coefficient $\gamma_0^{(n)}$ (cgs) and residual resistivity $\rho_n(0)$ approximated to $T = 0$, $n^{2/3}\frac{S}{S_F}$ calculated from Eq. (2), mean free path $l(0)$, BCS coherence length $\xi_0^{BCS}(0) = 7.95 \times 10^{-17}(n^{2/3}\frac{S}{S_F})(\gamma_0 T_c)^{-1}$, GLAC coherence length ξ_{GL}^{fv} [full value, (fv)], also calculated in the clean (c) and dirty (d) limit [60], London [$\lambda_L(0) = 1.33 \times 10^8 \gamma_0^{1/2}(n^{2/3}S/S_F)^{-1}$] and GLAG [$\lambda_{GL}(0)$] penetration lengths ($fv$), also calculated in the clean and dirty limit [60], Ginzburg-Landau parameter $\kappa_{GL}(0)$, critical temperature T_c and $T_c^\star$, thermodynamic critical field $H_c = 4.23\gamma_0^{1/2}T_c$, lower critical field $H_{c1} = H_c(0)\ln\kappa(\sqrt{2}\kappa)^{-1}$ in the limit $t = T/T_c \longrightarrow 0$, and the upper critical field H_{c2}.

$Lu_{5-\delta}Rh_6Sn_{18}$	$\gamma_0^{(n)}$ erg/cm^3 K^2	$\rho_n(0)$ $10^{-6}\times\Omega$ cm	$n^{2/3}\frac{S}{S_F}$ $10^{13}\times$cm^{-2}	$l(0)$ nm	$\xi(0)$ nm	$\lambda(0)$ nm	$\kappa(0)$	T_c K	$T_c^\star$ K	dH_{c2}/dT $10^4\times$G/K	H_c G	H_{c1} G	H_{c2} $10^4\times$G
Sample 1	467	4.9	2.3	1130	$\xi_0^{BCS}(0)=9.6$	$\lambda_L(0)=1240$		4.06	4.09	−1.62	373	10	5.2
					$\xi_{GL}^{fv}(0)=7.06$	$\lambda_{GL}^{fv}(0)=883$	$\kappa_{GL}^{fv}(0)=125$						
					$\xi_{GL}^{c}(0)=7.10$	$\lambda_{GL}^{c}(0)=880$	$\kappa_{GL}^{c}(0)=124$						
					$\xi_{GL}^{d}(0)=88.8$	$\lambda_{GL}^{d}(0)=70$	$\kappa_{GL}^{d}(0)=0.8$						
Sample 2	142	147	0.66	131	$\xi_0^{BCS}(0)=10.0$	$\lambda_L(0)=2401$		3.69	3.75	−1.73	229	1	5.3
					$\xi_{GL}^{fv}(0)=7.0$	$\lambda_{GL}^{fv}(0)=1744$	$\kappa_{GL}^{fv}(0)=245$						
					$\xi_{GL}^{c}(0)=7.4$	$\lambda_{GL}^{c}(0)=1691$	$\kappa_{GL}^{c}(0)=229$						
					$\xi_{GL}^{d}(0)=25.0$	$\lambda_{GL}^{d}(0)=405$	$\kappa_{GL}^{d}(0)=13$						

$Lu_5Rh_6Sn_{18}$ shown in Fig. 8 reveal the presence of (i) several Dirac conelike shapes (e.g., on $\Gamma - Z - \Sigma 1$ symmetry lines) and (ii) the pseudogap with almost zero TDOS at $\sim$−0.3 eV. The first unusual behavior, (i), is characteristic of the special class of nonsymmorphic materials [40] with the presence of Dirac cones and Dirac nodes; while depending on the filling level of the bands, the nonsymmorphic materials may also undergo Mott variable-range hopping effect [41,42] [the case (ii)] if the deep minimum in the d-electron DOSs would be located close to the Fermi level.

Figure 9 compares the ac mass susceptibility $\chi_{ac} = \chi' - i\chi''$ of sample 1 [panel (a)] and sample 2 (b), measured at different frequencies with amplitude $2 \times 1000/4\pi$ A/m (2 Oe) of the applied ac field. The maxima in $d\chi'/dT$ and $d\chi''/dT$ define the critical temperature T_c and/or $T_c^\star$. The components χ' and χ'' shown in Fig. 9(b) indicate a broad transition between the normal and superconducting states in sample 2; this signals that the inhomogeneous *high temperature* superconducting $T_c^\star$ phase is not well separated from the bulk superconducting one, giving $T_c^\star \approx T_c$. In contrast to this behavior, the χ_{ac} data shown for sample 1 in Fig. 9(a) signals the presence of an inhomogeneous superconducting $T_c^\star$ phase well separated from the bulk T_c phase, and both transitions are observed to be more narrow. One also notes the perfect diamagnetism of the full Meissner state with the expected value of $\chi' = -1/(4\pi d) \approx -8.5 \times 10^{-3}$ A m^2 kg^{-1} (emu/g) and mass density $d = 9.42$ g/cm^3 for both samples 1 and 2 at temperatures $T < T_c$ (cf. Fig. 9) [43]. Figure 10 displays the magnetization M vs B isotherms for sample 1 [panel (a)] and sample 2 [panel (b)]. The samples are diamagnetic with hysteresis loops in the superconducting state, representing the effect of vortex pinning. A very crude estimate gives the critical field $H_{c1} \approx 0.023$ T and $\sim$0.006 T for sample 1 and 2, respectively (230 and 60 G). The calculated critical fields H_{c1} are for sample 1 and 2 one order of magnitude smaller than those estimated experimentally (cf. Table III), however, the relation between the respective calculated quantities H_{c1}(sample1) > H_{c1}(sample2) matches the experimental data.

The magnetic data in Figs. 9 and 10 (chi_{ac} and M) show that samples 1 and 2 are diamagnetic in their normal state. The diamagnetic effect dominates the Pauli paramagnetism for $T > T_c$ and mostly results from Rh d-electron states (as results from DFT calculations) and Landau diamagnetism of the free electron gas (a Fermi surface effect). One can suppose that the electron states close to the Fermi surface are diamagnetically active, then even a weak effect should be related to the DOS at ϵ_F. A comparison of the mass ac susceptibility in the normal state between these two compounds (see Fig. 9) gives $|\chi'_{ac}|$ of sample 1 one order in magnitude larger than $|\chi'_{ac}|$ of sample 2, which is evidence that the enhanced superconductivity in $Lu_{5-\delta}Rh_6Sn_{18}$ is a result of the changed electronic structure at the Fermi level. The variation in DOS, depending on the sample stoichiometry, also significantly changes the temperature dependence of resistivity, as discussed below.

Figure 11 shows the specific heat of sample 1 [panel (a)] and sample 2 [panel (b)] at various magnetic fields (insets). As an attempt, the low-T C/T data at zero magnetic field have been approximated by a two-gap model. The two-gap scenario can be expected from the band structure calculations, which confirm the presence of various s, p, and d electronic states at the Fermi level, as Fig. 7 presents. Under the two-gap scenario the best fit is given by the expression:

$$\frac{C(T)}{T} = \gamma_0{}' + \beta' T^2 + \frac{1}{T}A\left[y\,\exp\left(-\frac{\Delta_1}{k_B T}\right) + (1-y)\,\exp\left(-\frac{\Delta_2}{k_B T}\right)\right], \quad (1)$$

with the parameters $\gamma_0' = 0.008$ J/mol K^2, $\beta' = 0.023$ J/mol K^4, $y = 0.95$, $\Delta_1/k_B = 12.6$ K, and $\Delta_2/k_B = 5.0$ K, respectively for sample 1. However, the approximation of Eq. (1) gives a very small contribution of the second band to the electronic specific heat data of sample 1 ($y \sim 0.95$), which causes the multiband model not to be clearly defined. The C/T data also can be well approximated by the one-gap scenario, where in Eq. (1) $y = 1$, then the fitting parameters γ_0' and β' are obtained similarly, and $\Delta/k_B = 11.4$ K, respectively. Our previous investigations of a number of similar quasiskutterudite

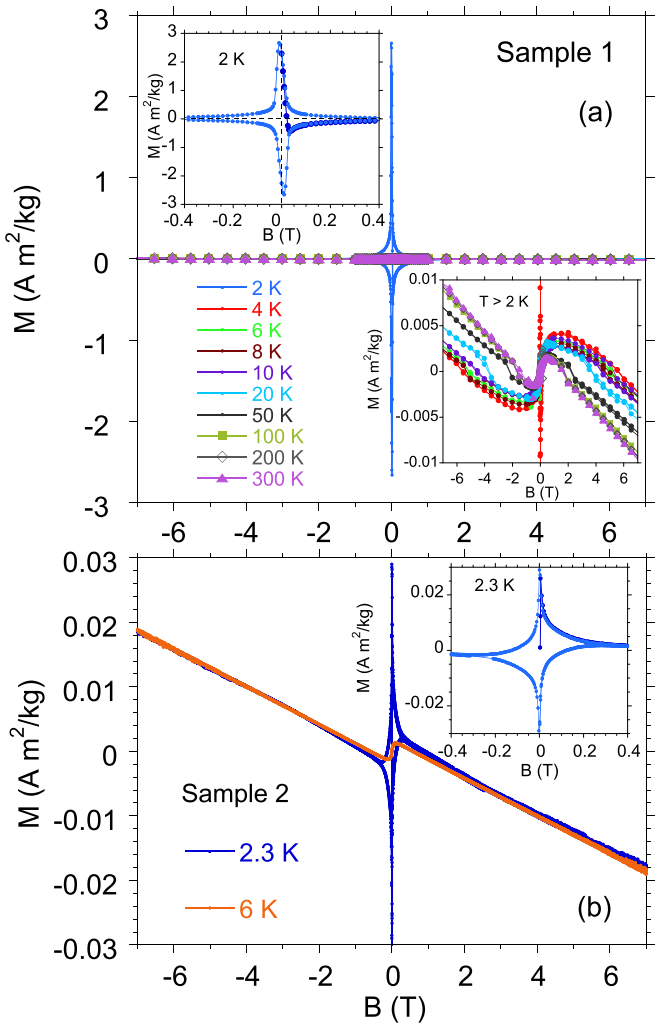

FIG. 10. The magnetization M isotherms vs magnetic field B for sample 1 [panel (a)] and sample 2 [panel (b)] at different temperatures [the used unit 1 A m^2/kg (SI) is equivalent to 1 emu/g (cgs)]. (a) The left inset shows the hysteresis loop at $T = 2$ K for the superconducting state of sample 1, the lower inset exhibits the diamagnetic behavior at various temperatures $T > 2$ K. The inset in panel (b) exhibits the hysteresis loop measured for sample 2 at $T = 2.3$ K.

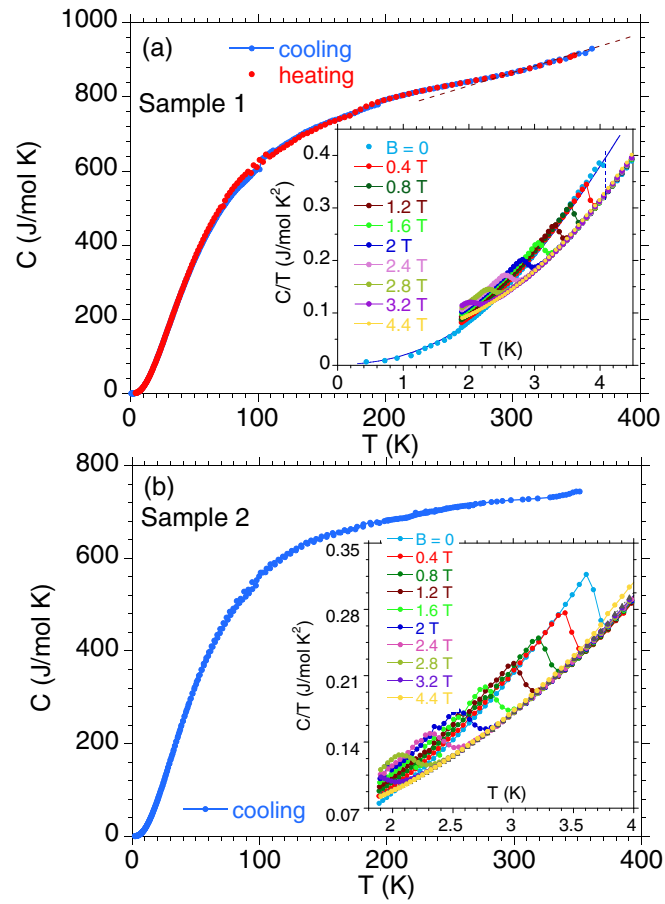

FIG. 11. (a) Temperature dependence of specific heat, $C(T)$, for sample 1, measured in the heating-cooling cycles. The inset displays $C(T)/T$ data in various magnetic fields. The dark blue line is the best fit of Eq. (1) to the $C(T)/T$ data in the temperature region $T < T_c$. (b) Temperature dependence of $C(T)$ for sample 2. The inset displays $C(T)/T$ data in various magnetic fields.

superconductors documented their multiband superconductivity [19,33], however, in the case of sample 1, the specific heat does not give an unambiguous answer, whether the system is a dirty one-gap or two-gap superconductor.

The normal-state electronic specific heat coefficient $\gamma_0^{(n)}$ and the lattice specific heat coefficient β were obtained for sample 1 at $T > T_c$ by a least-squares fit of the $C(T)/T$ data to $C(T)/T = \gamma_0^{(n)} + \beta T^2$, which provides $\gamma_0^{(n)} = 18$ mJ/mol K^2. The similar least-squares fit of the 3 T data gives a Sommerfeld parameter $\gamma_0^{(sc)} = 36.2$ mJ/mol K^2 in the superconducting state ($T < T_c$). The same least-squares analysis gives $\gamma_0^{(n)} = 5.5$ mJ/mol K^2 and $\gamma_0^{(sc)} = 47.6$ mJ/mol K^2 ($B = 3$ T), respectively, for sample 2. For a classic BCS superconductor with a Debye lattice, the normal state would appear as a straight line $C/T = \gamma_0^{(n)} + \beta T^2$, and the electronic term would vanish exponentially at low temperatures in the superconducting state, so that below about $\sim T_c/7$ only the lattice specific heat contribution should survive. Therefore the initial slopes of both curves $C^{(n)}/T$ obtained for $T > T_c$ ($B = 0$) and $C^{(sc)}/T$, measured under magnetic fields $B > B_c$ at $T < T_c(0)$, should be equal. This is not the case here. The possible γ_0 discrepancies could be addressed to a vortex effect. For a classic isotropic s-wave superconductor (e.g., $Nb_{77}Zr_{23}$ [44]), the specific heat at $T < T_c$ is dominated by that of the vortex cores, the number of which is proportional to the field. As a result, one observes at $T \to 0$ a field dependence of $\gamma_0^{(sc)}$. Similar $\gamma_0(H)$ behavior was also reported for other skutteruditelike superconductors ($R_3M_4Sn_{13}$ [45–47], $Lu_5Rh_6Sn_{18}$, $Y_5Rh_6Sn_{18}$ [48,49], and $Sc_5Rh_6Sn_{18}$ [50]). For example, $\gamma_0^{(sc)}(H)$ for $Lu_5Rh_6Sn_{18}$ and $Y_5Rh_6Sn_{18}$ is continuously increasing from a few mJ/mol K^2 in the normal state ($T > T_c$ and $H = 0$), up to the value of about 60 mJ/mol K^2 under $H = 5$ T at $T = 0.7$ K. A linear increase in $\gamma_0^{(sc)}(H)$ was obtained for $Lu_5Rh_6Sn_{18}$, while for $Y_5Rh_6Sn_{18}$ $\gamma_0^{(sc)}(H) \sim H^{1/2}$ [49]. Based on these results, $Lu_5Rh_6Sn_{18}$ was interpreted as a BCS superconductor with an isotropic gap, while its $Y_5Rh_6Sn_{18}$ equivalent has an anisotropic gap with a node. The field increased $\gamma_0^{(sc)}$ is also

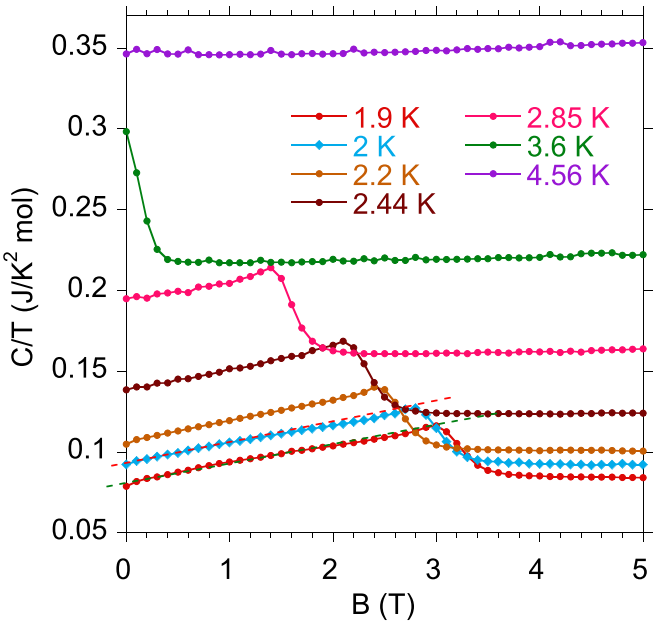

FIG. 12. Heat capacity C as a function of magnetic field B at constant temperatures T for sample 2. Similar behavior was observed for sample 1.

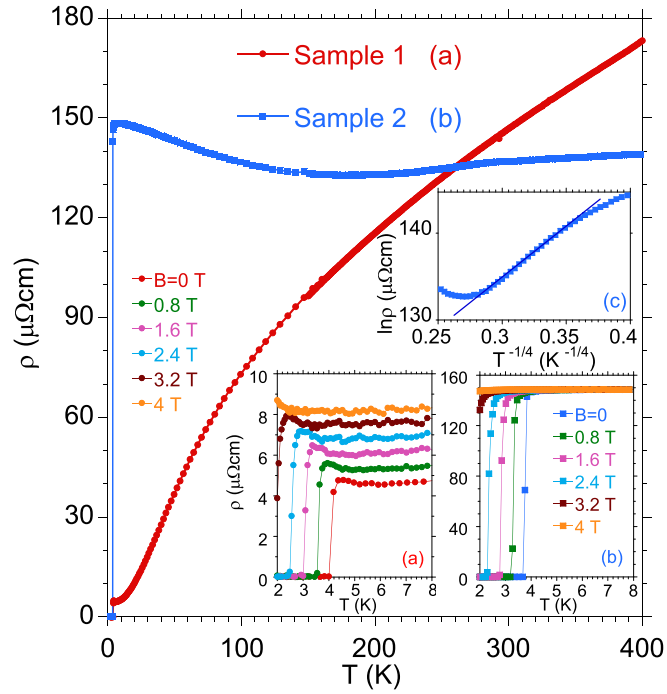

FIG. 13. Electrical resistivity $\rho(T)$ for sample 1 and sample 2. The lower insets show $\rho(T)$ at various externally applied fields for sample 1 and 2, respectively. Inset (c) displays the resistivity data for sample 2 in coordinates $\ln\rho = f(T^{-1/4})$. Blue line approximates the linear $\ln\rho$ vs $T^{-1/4}$ behavior in the temperature range between 60 K and 160 K.

strong evidence in favor of gap anisotropy or different gaps on different sheets of the Fermi surface, like in MgB_2. This scenario, however, seems to be unlikely for a $Lu_5Rh_6Sn_{18}$ superconductor. In Fig. 11, the specific heat of sample 1 exhibits a change of slope in $C(T)$ at about 300 K.This phenomenon is most likely related to the process of lattice relaxation and also was observed in a similar T region for the isostructural $Y_5Rh_6Sn_{18}$ quasiskutterudite system [28]. Figure 12 shows the specific heat isotherms $C_T(B)$ as a function of magnetic field B, which for temperatures $T < T_c$ exhibit a clear kink at the critical field H_{c2} and linear behavior under the fields lower than H_{c2}. This behavior is usually attributed to the s-wave one-band superconductivity.

Figure 13 shows the resistivity of sample 1 and sample 2. For both samples, the resistivity drop indicates the superconducting transition at $T_c^\star$ ($T_c^\star \gtrapprox T_c$, see Table III). The lower insets display the resistivity for samples 1 and 2 at various applied fields, while the upper inset shows $\ln\rho$ vs $T^{-1/4}$ dependence for sample 2. As shown in Fig. 13, the characteristics $\rho(T)$ in the *normal metallic state* are for these two samples quite different, for sample 1 the $\rho(T)$ plot is typical for metals, while the resistivity of the off-stoichiometric sample 2 indicates its semimetallic nature and exhibits a negative temperature coefficient (TCR) $d\rho/dT < 0$ in a large temperature range $T_c < T < 160$ K. However, this unusual increase in ρ with decreasing T does not exhibit a linear change, as could be expected for strongly disordered alloys [51], nor does it obey an activated law, while for $(60 < T < 160)$ K $\rho(T)$ obeys Mott's law $\rho \propto \exp[(\frac{\Delta_M}{k_B T})^{1/4}]$, known as Mott variable-range hopping effect [41] (Δ_M characterizes the pseudogap in the band structure near the Fermi level). In the case of metals, when a conduction and valence band overlap slightly giving a finite DOS at the Fermi energy, a *pseudogap* or minimum in the DOS is expected, as first suggested by Mott [42]. When the overlap increases, the states at ϵ_F are delocalized, and a metal-insulator transition of Anderson type is possible; at the limit of weak localization, conduction by hopping according to $\sigma \propto \exp[(-\frac{\Delta_M}{k_B T})^{1/4}]$ will occur in disordered materials. An agreement with Mott variable-range hopping behavior was observed, e.g., for some d-electron semiconducting Heusler alloys (cf. ZrNiSn and TiNiSn [52–54]) and Ce_5RuGe_2 [55]. The *ab initio* calculations predict for stoichiometric $Lu_5Rh_6Sn_{18}$ a pseudogap with a minimum in DOSs at $\sim$−0.3 eV due to interband hybridization effect (cf. Fig. 7). Previously, for similar $R_3Co_4Sn_{13}$ quasiskutterudites ($R =$ La [39] or Ce [38]) we documented that even a small number of vacancies can shift the pseudogap calculated at similar binding energies of $\sim$−0.3 eV towards the Fermi level; simultaneously, the presence of defects may reduce this pseudogap after its shift to ϵ_F (this is characteristic of SC Kondo insulators; see, e.g., Ref. [56]). We expect a similar band structure effect for the off-stoichiometry sample 2, which as a consequence of vacancies exhibits abnormal semimetallic $\rho(T)$ behavior with accompanying Mott variable-range hopping effect in its metallic state. The TDOS calculations done for $Lu_{5-\delta}Rh_6Sn_{18}$ with Lu deficiency (simulated by vacancies located at Lu sites) should better approximate the band structure of the experimental compositions and provide more information about the shift of the pseudogap in DOS towards the Fermi level. We therefore carried out similar DFT calculations for $Lu_{4.5}Rh_6Sn_{18}$ with the stoichiometry more close to that obtained from microanalysis. The *ab initio* calculations documented the shift of pseudogap in TDOS of $Lu_{4.5}Rh_6Sn_{18}$

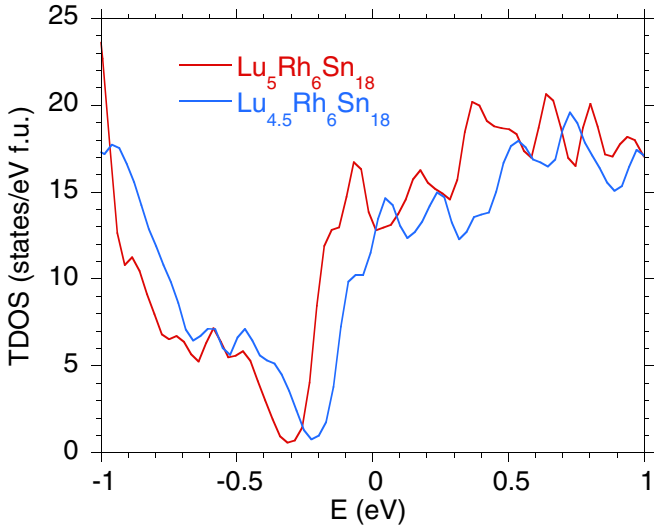

FIG. 14. The comparison of TDOS for $Lu_5Rh_6Sn_{18}$ and $Lu_{4.6}Rh_6Sn_{18}$ near the Fermi level.

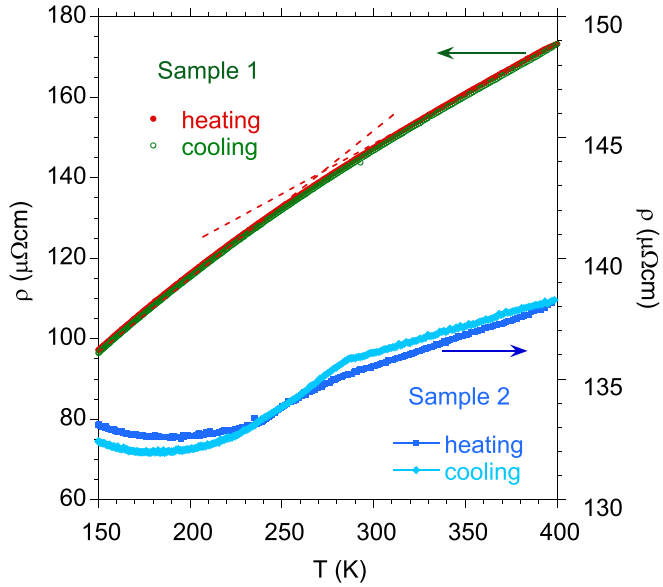

FIG. 15. Electrical resistivity in cooling/heating cycles for sample 1 and sample 2, between 150 K and 400 K.

by 0.1 eV towards ϵ_F in comparison to the stoichiometric variant 5-6-18, as shown in Fig. 14, while the energies of the SO Lu $4f^{7/2}$ and $4f^{5/2}$ states were not changed. The calculations did not take into account the Sn vacancies, which could significantly contribute to a greater energy shift of the pseudogap in TDOS towards ϵ_F (cf. Ref. [39]). Within such a scenario the resistivities shown in Fig. 13 well correlate with the specific heat data in Fig. 11. Namely, sample 1 with a hybridization pseudogap in DOS at -0.3 eV has a good metallicity, characterized by small *normal state residual resistivity* $\rho_n(0) \sim 5\ \mu\Omega$ cm, while $\rho_n(0)$ of the off-stoichiometric sample 2 is about two orders of magnitude larger due to a possible shift of the pseudogap towards ϵ_F. Simultaneously, the electronic specific heat coefficient $\gamma_0^{(n)}$ obtained in the normal state for sample 1 is 18 mJ/mol K^2 ($\equiv$467 erg/cm^3 K^2), while a value of $\gamma_0^{(n)} = 5.5$ mJ/mol K^2 ($\equiv$142 erg/cm^3 K^2) for semimetallic sample 2 is much smaller. Such divergent behaviors seen in two different $Lu_{5-\delta}Rh_6Sn_{18}$ samples result from their different real electronic structures near ϵ_F generated by vacancies and accompanying changes in the density of states $2N(\epsilon_F)$ (cf. Table III). It is worth it to note our earlier paper [57], where we documented different field skutterudite $CeOs_4Sb_{12}$ single-crystal specimens—all obtained in one technological process by flux method, a spectrum of various conductivities from metallic to semiconducting, as a result of the changed number of vacancies in the Sb sublattices, depending on which crystal was measured (cf. Fig. 2 in Ref. [57]). Then, one can comment that the temperature dependence of ρ, previously reported by Zhang *et al.* [58] for single crystalline $Lu_5Rh_6Sn_{18}$, is similar to that obtained for sample 2. Both the band structure properties of $Lu_5Rh_6Sn_{18}$ near the Fermi level from *ab initio* calculations, as well as its various electric transport properties—depending on the stoichiometry of this compound—support the assumption that the semimetallic behavior and negative TCR effect in $\rho(T)$ reported for single crystals of $Lu_5Rh_6Sn_{18}$ [58] also result from the off-stoichiometry effect.

The low-T resistivity of sample 1 exhibits a field induced positive magnetoresistivity (MR) in the normal metallic state, and the isothermal increase in ρ_T vs B is linear, $\rho_T = \varrho B$, with coefficient $\varrho \cong 1\ \mu\Omega$ cm/T, as is shown in inset (a), Fig. 13. Similar positive MR effect has been previously documented for a series of metallic (e.g., $Y_3Ir_4Ge_{13}$ [59]) or superconducting ($La_3M_4Sn_{13}$ [37]) quasiskutterudites and was attributed to the Coulomb interactions between the d electrons of transition metal M which dominate the field-dependent electronic transport in these materials. In Fig. 7 the DFT band structure calculations confirm the d-band character of the conduction electrons, which dominate the DOS at ϵ_F. The field induced magnetoresistivity effect is, however, not observed for the off-stoichiometry $Lu_{4.6}Ru_6Sn_{18}$. For this semimetallic sample with the pseudogap expected at the Fermi level, the d electrons correlation effect is not possible.

Figure 15 shows the cooling-heating evolution of $\rho(T)$ data in the temperature range $150 < T < 400$ K. A clear kink in ρ at about 290 K and a hysteresis is observed for sample 2, while sample 1 shows only a weak change in the slope of $\rho(T)$ without any hysteresis at this temperature. The phenomenon seen in the electrical resistivity is most likely related to the process of thermal lattice relaxation and is also evidenced by the specific heat data in Fig. 11.

C. Superconductivity of $Lu_{5-\delta}Rh_6Sn_{18}$ in the presence of atomic disorder: Experimental results and comparison with BCS theory

Now we analyze the experimental data: The coefficient of the electronic heat capacity $\gamma_0^{(n)}$, normal state resistivity $\rho_n(0)$ approximated to $T = 0$, and the measured critical-field slopes near T_c with predictions of the Ginzburg-Landau-Abricosov-Gorkov (GLAG) theory of type-II superconductivity, to obtain the parameters characteristic of the superconducting and normal state of the investigated samples [e.g., coherence length $\xi(0)$, penetration depth $\lambda(0)$, GLAC parameter κ, electronic mean free path $l(0)$, and the critical fields $H_c(0)$ and $H_{c1}(0)$].

According to Ref. [60], all parameters are calculated as a *full value*, or at the clean ($\xi \ll l$) and dirty limit ($\xi \gg l$), and are listed in Table III. Under the GLAG theory [61] the slope of $\frac{dH_{c2}}{dT}$ at T_c in the G/K units is

$$-\left.\frac{dH_{c2}}{dT}\right|_{T=T_c} = \left[9.55\times 10^{24}\gamma_0^2 T_c\left(n^{2/3}\frac{S}{S_F}\right)^{-2} + 5.26\times 10^4\gamma_0\rho_n\right][R(\lambda_{tr})]^{-1}, \quad (2)$$

where n is the density of conduction electrons per cm^{-3}, S/S_F is the ratio of the real Fermi surface S to the surface $S_F = 4\pi(3\pi^2 n)^{3/2}$ of the free electron gas, and the Gorkov function $R(\lambda_{tr}) \approx 1$ for $\lambda_{tr} \longrightarrow 0$ ($\lambda_{tr} \sim \xi(0)/l(0) = 5.51\times 10^{-21}\rho_n(n^{2/3}S/S_F)(\gamma_0 T_c)^{-1} \approx 0$ for $Lu_5Rh_6Sn_{18}$). Equation (2) allows one to estimate the value of $n^{2/3}\frac{S}{S_F} = 2.3\times 10^{13}$ cm^{-2} for sample 1 and 0.66×10^{13} cm^{-2} for sample 2, respectively [62–64]. Then, the electronic mean free path $l(0) = 1.27\times 10^4[\rho_n(n^{2/3}S/S_F)]^{-1} = 1130$ nm is estimated much larger for sample 1 in comparison to $l(0) = 85$ nm obtained for sample 2, while the Ginzburg-Landau coherence length (full value)

$$\xi_{GL}^{fv} = \left[2.90\times 10^{32}(T_c\gamma_0)^2\left(n^{2/3}\frac{S}{S_F}\right)^{-2} + 1.60\times 10^{12}\rho_n\gamma_0 T_c\right]^{-1/2}[R(\lambda_{tr})]^{1/2}(1-t)^{-1/2} \quad (3)$$

is ~7 nm for both samples. From the Ginzburg-Landau relation $\mu_0 H_{c2}(0) = \Phi_0/2\pi\xi_{GL}^2(0)$ $\xi_{GL}(0) = 8$ nm, where $\Phi_0 = h/2e = 2.068\times 10^{-15}$ T m^2 is the flux quantum. The relation $\xi_{GL}^{fv} \ll l(0)$ predicts a clean limit in superconductivity of $Lu_5Rh_6Sn_{18}$ (sample 1 and 2), although the atomic disorder is evident in both samples. The BCS coherence length $\xi_0^{BCS} = 7.95\times 10^{-17}(n^{2/3}S/S_F)(\gamma_0 T_c)^{-1} \approx 10$ nm is very similar to the value of ξ_{GL}^{fv}.

The Ginzburg-Landau penetration depth

$$\lambda_{GL}^{fv} = \left[8.77\times 10^{15}\gamma_0\left(n^{2/3}\frac{S}{S_F}\right)^{-2} + 4.83\times 10^{-5}\rho_n T_c^{-1}\right]^{1/2} \times [R(\lambda_{tr})]^{-1/2}(1-t)^{-1/2} \quad (4)$$

(see Table III) gives GLAC parameter

$$\kappa_{GL}^{fv} \equiv \lambda_{GL}(0)/\xi_{GL}(0) = \left[1.60\times 10^{24}T_c\gamma_0^{3/2}\left(n^{2/3}\frac{S}{S_F}\right)^{-2} + 8.78\times 10^3\gamma_0^{1/2}\rho_n\right] \times [R(\lambda_{tr})]^{-1} \gg 1, \quad (5)$$

which determines $Lu_{5-\delta}Rh_6Sn_{18}$ (sample 1 and 2) to be a superconductor of type II. Our analysis also includes the dirty limit, where the GLAG parameter $\kappa_{GL}^d = 7.49\times 10^3\gamma_0^{1/2}\rho_n$ [60] is 0.8 or 13 for samples 1 and 2, respectively, i.e., a much smaller value of κ_{GL}^d than expected for a superconductor of type II. However, $\kappa_{GL}^d \sim 0.8$ for sample 1 is close to $1/\sqrt{2}$ that separates the superconductivity of type I ($\kappa < 1/\sqrt{2}$) and type II ($\kappa > 1/\sqrt{2}$). Then, the critical field $H_c^d(0) = \frac{H_{c2}}{\sqrt{2}\kappa_{GL}^d} = 4.7$ T would be estimated for sample 1

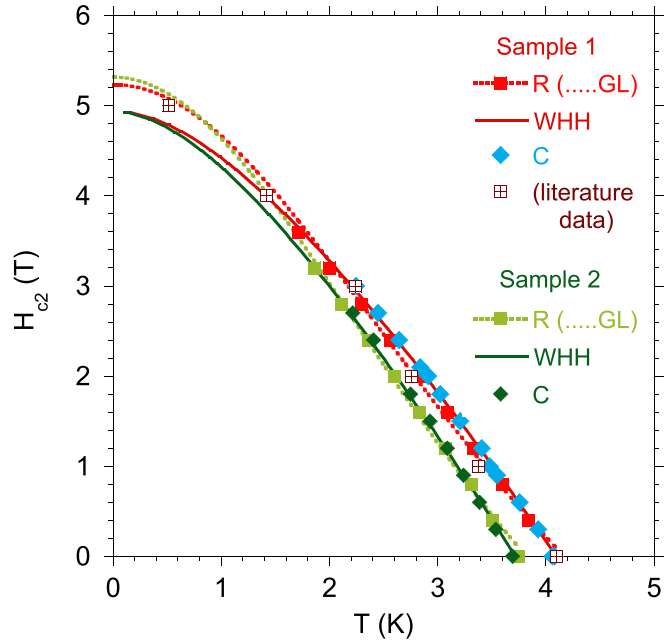

FIG. 16. The upper critical field H_{c2} vs T for $Lu_{5-\delta}Rh_6Sn_8$ (sample 1 and 2). The points are determined from specific heat $C_B(T)$ and/or $C_T(B)$ (filled squares) and from resistivity $\rho_B(T)$ (filled diamonds) measurements. The brown open squares are the data from Ref. [58] for comparison. The $H-T$ data are well approximated by GL equation (red dotted curve for sample 1 and light green dotted line for sample 2). For both samples, 1 and 2, $T_c^\star$ (filled squares) is measured slightly larger by ~0.02 K than T_c (filled diamonds) for $B = 0$. The solid red and dark green curves are obtained by the single band WHH model using Eq. (11).

almost equal to its critical field $H_{c2} = 5.2$ T, which drastically deviates from the experiment (cf. Table III). In the clean limit this expression, however, gives $H_c^c(0) \approx 0.03$ T (300 G) in accordance with an alternate estimate of $H_c(0) = 0.0373$ T (373 G), based on the expression $H_c(0) = 4.23T_c\sqrt{\gamma_0}$ (as shown by Table III). For sample 2 $\kappa_{GL} \gg 1/\sqrt{2}$ for both the clean and dirty limits and $H_c(0)$ is calculated 0.02 T (clean limit) or 0.23 T (dirty limit), respectively. It can therefore be suggested that the $Lu_{5-\delta}Rh_6Sn_{18}$ samples are largely homogeneous, however, with possible intersite and/or displacive [33] atomic disorder present in both samples (1 and 2) or even with fluctuations in composition as was documented for sample 1. It is worth it to note that only in the moderate disorder regime, the characteristic relation $\xi_{GL}^d(0) = \sqrt{\xi_0^{BCS}l(0)}$ is roughly satisfied for both samples.

The observed relation $\xi_0 \ll l(0)$ also justifies that $H_{c2}(T)$ cannot be well approximated with the Werthamer-Helfand-Hohenberg (WHH) [61,65] or Maki-de Gennes [66] theories for a dirty superconductor (cf. Fig. 16). The microanalysis, however, confirms the presence of moderate atomic disorder in both samples and shows a periodic fluctuation in composition on a long distance of about 25 μm for sample 1 [67]. (i) From the local atomic disorder results the presence of the *high temperature phase* $T_c^\star$, the effect $T_c^\star - T_c \approx 5\times 10^{-2}$ K is weak but experimentally confirmed for sample 1 and 2. (ii) Simultaneously, the enhanced T_c of sample 1 by about 0.4 K

with respect to T_c of sample 2 can be due to the periodic inhomogeneity effect. Very similar enhancing of the superconductivity by fluctuation of the composition was recently documented and discussed for $Y_5Rh_6Sn_{18}$ [19] within the Gastiasoro and Andersen theoretical model [18].

The BCS theory gives a relation between T_c, $\langle\omega\rangle$, and the interaction strength $N(\epsilon_F)U$

$$T_c = 1.14\langle\omega\rangle \exp[-1/(N(\epsilon_F)U)]. \tag{6}$$

The equivalent of $N(\epsilon_F)U$ is approximately [68]

$$N(\epsilon_F)U \rightarrow \frac{\lambda - \mu^\star}{1+\lambda}, \tag{7}$$

where $\mu^\star$ is the Coulomb pseudopotential of Morel and Anderson [69],

$$\mu^* = \frac{N(\epsilon_F)U}{1 + N(\epsilon_F)U \ln(E_B/\omega_0)}, \tag{8}$$

and electron-phonon coupling parameter [70,71]

$$\lambda = \frac{N(\epsilon_F)\langle I^2\rangle}{M_A\langle\omega^2\rangle}. \tag{9}$$

In Eqs. (6)–(9) $\langle I^2\rangle$ represents the square of the electronic matrix element of electron-phonon interactions averaged over the Fermi surface, $\langle\omega\rangle \sim \theta_D/1.2$ is an average phonon frequency, $N(\epsilon_F)$ is a density of states at the Fermi energy in states per eV and per spin, M_A is the atomic mass, E_B is the electronic bandwidth, and ω_0 is the maximum phonon frequency.

From Eqs. (8) and (7), one is able to determine [19]

$$N(\epsilon_F)U = \frac{-[2+\lambda(1-x)] + [\lambda^2(1+x)^2 + 4\lambda + 4]^{1/2}}{2x(1+\lambda)}, \tag{10}$$

where $x = \ln(E_B/\omega_0)$. For sample 1 $T_c = 4.06$ K, $T_c^\star = 4.09$ K, $\theta_D = 149$ K, and $E_B = 5$ eV (cf. Fig. 7), then Eq. (6) allows us to estimate $N(\epsilon_F)U = 0.2815$ for the T_c bulk phase and $[N(\epsilon_F)U]^\star = 0.2821$ for the inhomogeneous $T_c^\star$ phase, respectively. From Eq. (10) one can calculate $N(\epsilon_F)U$ as a function of λ, for the T_c and $T_c^\star$ phase, respectively, and then compare them with the appropriate $N(\epsilon_F)U$ quantities obtained experimentally from Eq. (6). The proposed self-consistent procedure gives the best agreement between calculated and experimentally obtained $N(\epsilon_F)U$ for $\lambda = 0.53(4)$ in the case of the bulk T_c phase and $\lambda^\star = 0.54(0)$ for the *disordered* $T_c^\star$ phase, respectively. The λ and $\lambda^\star$ are, however, very similar, which again suggests that $Lu_5Rh_6Sn_{18}$ is largely homogeneous. Similar self-consistent action gives more similar $\lambda = 0.52(0)$ and $\lambda^\star = 0.52(2)$ for sample 2. The λ parameter obtained self-consistently can be verified, e.g., by the analysis of the normal-state specific heat in a standard way (at $T < T_c$ and under magnetic field B) according to the expansion $C(T \rightarrow 0) = \gamma_0 T + C_{ph}$, where in the first term $\gamma_0 = \frac{\pi^2 k_B^2 N_A}{3} 2N(\epsilon_F)(1+\lambda)$ the correction factor $(1+\lambda)$ remains as a consequence of the different electron-phonon renormalizations of the band structure density of states at the Fermi level. The second term is the low-temperature expansion of the lattice specific heat. For $2N(\epsilon_F) = 11.5$ states/eV f.u. from DFT calculations and $\lambda = 0.53(4)$, the estimated $\gamma_0 = 41.72$ mJ/mol K^2 matches well the experimental data ($\gamma_0^{(sc)}$) measured in the superconducting state under magnetic field namely, 47.6 mJ/mol K^2 for sample 2 and 36.2 mJ/mol K^2 for sample 1. The DOS renormalized by electron-phonon coupling explains partially the enhanced Sommerfeld coefficient, however, for correct interpretation one needs to consider the field effect on $\gamma_0^{(sc)}$ too.

The dotted curves in Fig. 16 represent the best fit of the $H_{c2}(T)$ data by the Ginzburg-Landau (GL) formula: $H_{c2}(T) = H_{c2}(0)\frac{1-t^2}{1+t^2}$, where $H_{c2}(0)$ is the upper critical field at $T = 0$. The $H - T$ data for samples 1 and 2 are well described by the GL equation with similar $H_{c2}(0) \approx 5.3$ T. For comparison, Fig. 16 also displays the respective temperature dependencies of H_{c2} derived within the WHH model, which includes orbital and Zeeman pair breaking [61,65]. For a single band superconductor in a dirty limit, the model yields the well-known WHH formula for the upper critical field:

$$H_{c2}(0) = -0.69T_c \left.\frac{dH_{c2}}{dT}\right|_{T=T_c}. \tag{11}$$

For our samples the slope $\mu_0\frac{dH_{c2}(T)}{dT} = -1.63$ T/K (sample 1) or -1.69 T/K for sample 2. Within the WHH theory $H_{c2}(0) \cong 4.93$ T is for both samples $\sim$0.4 T smaller than that obtained experimentally and approximated by the GL expression. Different mechanisms have been proposed to explain this behavior, such as strong coupling effects, multiband electronic structure, and/or disorder [33,72]. In the case of the $Lu_{5-\delta}Rh_6Sn_{18}$ samples, the multiband model seems to be probable, considering the more complicated band structure of these compounds with the presence of various electronic states at the Fermi level, as shown in Fig. 7. To confirm this hypothesis, the $H_{c2}(T)$ was calculated according to the Gurevich [73] theory, which adopts the Eilenberger and Usadel equations for a two-band dirty superconductor. Within the model, the reduced magnetic field $h = H_{c2}D_1/2\Phi_0 T$ is a solution of the nonlinear equation

$$a_0[\ln t + U(h)][\ln t + U(\eta h)] + a_2[\ln t + U(\eta h)] + a_1[\ln t + U(h)] = 0, \tag{12}$$

where $U(x) \equiv \psi(x+1/2) - \psi(1/2)$, $\psi(\ldots)$ is the digamma function, and $\eta = D_2/D_1$ is the ratio of the intraband electron diffusivities D_1 and D_2. The parameters $a_{0,1,2}$ can be expressed by the intra- and interband BCS superconducting coupling constants λ_{11}, λ_{22}, λ_{12}, and λ_{21}. However, fitting the solution of Eq. (12) to $H_{c2}(T)$ data for $Lu_{5-\delta}Rh_6Sn_{18}$ gives $\eta \approx 1$. In this case Eq. (12) reduces to

$$\ln t + U(h) = 0, \tag{13}$$

which is the standard Maki-de Gennes equation for $H_{c2}(T)$ in single band dirty superconductors [66], which indicates that the role of the second band is practically negligible in the superconductivity of the $Lu_{5-\delta}Rh_6Sn_{18}$ samples.

IV. CONCLUDING REMARKS

The main goal of our comprehensive research of various quasiskutterudites was to document experimentally and interpret the impact of an atomic disorder characteristic of these materials on enhancement of their superconductivity. Since varying amounts of disorder may be present in these materials, and because the superconducting state is effected

by various structural defects, vacancies, and/or by doping, it is important to precisely identify them and to understand the role of widely understood defects on the superconductivity. There are several experimental approaches to study the disorder-induced superconductivity in the skutterudite-related cubic $R_3M_4Sn_{13}$-type [15,74] or tetragonal $R_5M_6Sn_{18}$-type compounds [19,33], where $R =$ Ca and La, or Y and Lu, respectively (see also Ref. [75]). One of them is to measure the change of the superconducting transition temperature T_c with well controlled disorder of the sample, which also can be artificially introduced by doping. Recently, we documented the structural defects, like disorder caused by static displacements of atoms in cages, local disorder due to antisite positions of the neighboring atoms or disorder resulting from doping; all these defects contribute to the increase in T_c, observed as $T_c^\star$. The coexisting *bulk* T_c phase and the *high-temperature* $T_c^\star$ phase and the $T_c^\star > T_c$ behavior fit well the mechanism of disorder-generated T_c enhancement, very recently proposed by Gastiasoro and Andersen [18]. In accordance with this theoretical model, the structural defects at a low concentration level can be understood as the elemental impurity effect, giving the basis for interpretation of the increase in T_c at the level of the dilute disorder case. However, the effect of stronger fluctuations in both atomic disorder and composition in $Y_{5-x}Ca_xRh_6Sn_{18}$ ($x > 2$, [19]) leads to a significant increase in T_c as a result of stoichiometry fluctuations, and it is well interpreted by the Gastiasoro and Andersen model of dense disorder in a conventional one-band superconducting system. Similar enhancing of superconductivity by the increase in atomic disorder is also observed for the $Lu_{5-\delta}Rh_6Sn_{18}$ compounds, which confirms that this anomalous behavior is characteristic of the family of skutterudite-related compounds. The microanalysis documented that sample 2 is a homogeneous system with small nanoscale atomic disorder, characterized by the transition to the superconducting state at $T_c = 3.7$ K, while sample 1 exhibits both nanoscale inhomogeneity and long-range fluctuations in composition, and its $T_c^\star \sim 4.1$ K. If one treats sample 2 as a reference compound for sample 1, then the $T_c^\star > T_c$ relation can be interpreted under the Gastiasoro and Andersen model as the effect of increased disorder in sample 1.

Our systematic research on the series of quasiskutterudites allowed us to propose a phenomenological model that explains the $T_c^\star > T_c$ behavior, based on the documented experimentally larger lattice stiffening in the $T_c^\star$ phase with respect to the bulk effect below T_c. For various quasiskutterudites investigated under pressure we always found $|\frac{dT_c^\star}{dP}| > |\frac{dT_c}{dP}|$ and accompanying $T_c^\star > T_c$ behavior; both relations are characteristic of these materials [75,76]. Considering that the P dependence on θ_D is given by the Grüneisen parameter $\gamma_G = -\frac{d\ln\theta_D}{d\ln V}$ and determines the lattice stiffening, we documented experimentally $\gamma_G^\star > \gamma_G$ for $T_c^\star$ and T_c phases, respectively (e.g., for $Y_5Rh_6Sn_{18}$ doped with Ca [19] and for $La_3Rh_4Sn_{13}$ [75]). The relationship between γ_G and T_c seems to be correct for all disordered skutterudite-related superconductors as well as for the filled skutterudite $PrOs_4Sb_{12}$ superconductor [77]. This is one of the most interesting results obtained for this intriguing single crystal of $PrOs_4Sb_{12}$, namely the observation of two various superconducting transitions at T_c and $T_c^\star$, and the measured value of $|\frac{dT_c^\star}{dP}|$, which is ~20% larger than $|\frac{dT_c}{dP}|$ [77]. For the family of quasiskutterudite superconductors our research has confirmed that the coupling λ parameter correlates with γ_G and always $\lambda^\star > \lambda$ [75]; this is also the case for $Lu_{5-\delta}Rh_6Sn_{18}$.

ACKNOWLEDGMENTS

M.M.M. acknowledges support by the National Science Centre (Poland) under Grant No. DEC-2018/29/B/ST3/01892. This research used resources of the Advanced Photon Source, a U.S. Department of Energy (DOE) Office of Science User Facility, operated for the DOE Office of Science by Argonne National Laboratory under Contract No. DE-AC02-06CH11357. Extraordinary facility operations were supported in part by the DOE Office of Science through the National Virtual Biotechnology Laboratory, a consortium of DOE national laboratories focused on the response to COVID-19, with funding provided by the Coronavirus CARES Act. Certain commercial equipment, instruments, or materials (or suppliers, or software,...) are identified in this paper to foster understanding. Such identification does not imply recommendation or endorsement by the National Institute of Standards and Technology, nor does it imply that the materials or equipment identified are necessarily the best available for the purpose. All reported uncertainties are statistical on a 1-σ level. We are grateful to Prof. Ewa Talik (University of Silesia in Katowice) for the measurement of the VB XPS spectrum of metallic Rh, using PHI 5700 ESCA spectrometer described in Sec. II.

[1] P. W. Anderson, J. Phys. Chem. Solids **11**, 26 (1959).
[2] B. T. Matthias, H. Suhl, and E. Corenzwit, Phys. Rev. Lett. **1**, 92 (1958).
[3] G. Chanin, E. A. Lynton, and B. Serin, Phys. Rev. **114**, 719 (1959).
[4] H. Suhl and B. T. Matthias, Phys. Rev. **114**, 977 (1959).
[5] A. A. Golubov and I. I. Mazin, Phys. Rev. B **55**, 15146 (1997).
[6] A. M. Goldman and N. Markovic, Phys. Today **51**, 39 (1998).
[7] M. V. Feigel'man, L. B. Ioffe, V. E. Kravtsov, and E. A. Yuzbashyan, Phys. Rev. Lett. **98**, 027001 (2007).
[8] F. Steglich, J. Aarts, C. D. Bredl, W. Lieke, D. Meschede, W. Franz, and H. Schäfer, Phys. Rev. Lett. **43**, 1892 (1979).
[9] N. D. Mathur, F. M. Grosche, S. R. Julian, I. R. Walker, D. M. Freye, R. K. W. Haselwimmer, and G. G. Lonzarich, Nature (London) **394**, 39 (1998).
[10] M. B. Maple, P.–C. Ho, V. S. Zapf, N. A. Frederick, E. D. Bauer, W. M. Yuhasz, F. M. Woodward, and J. W. Lynn, J. Phys. Soc. Jpn. Suppl. **71**, 23 (2002).

[11] R. Vollmer, A. Faißt, C. Pfleiderer, H. v. Löhneysen, E. D. Bauer, P.-C. Ho, V. Zapf, and M. B. Maple, Phys. Rev. Lett. **90**, 057001 (2003).

[12] G. Seyfarth, J. P. Brison, M.-A. Méasson, D. Braithwaite, G. Lapertot, and J. Flouquet, Phys. Rev. Lett. **97**, 236403 (2006).

[13] M.-A. Méasson, D. Braithwaite, G. Lapertot, J.-P. Brison, J. Flouquet, P. Bordet, H. Sugawara, and P. C. Canfield, Phys. Rev. B **77**, 134517 (2008).

[14] A. Bianchi, R. Movshovich, M. Jaime, J. D. Thompson, P. G. Pagliuso, and J. L. Sarrao, Phys. Rev. B **64**, 220504(R) (2001).

[15] A. Ślebarski, M. Fijałkowski, M. M. Maśka, M. Mierzejewski, B. D. White, and M. B. Maple, Phys. Rev. B **89**, 125111 (2014).

[16] M. Leroux, V. Mishra, J. P. C. Ruff, H. Claus, M. P. Smylie, Ch. Opagiste, P. Rodière, A. Kayani, G. D. Gu, J. M. Tranquada, W.-K. Kwok, Z. Islam, and U. Welp, Proc. Natl. Acad. Sci. USA **116**, 10691 (2019).

[17] B. M. Andersen, A. Melikyan, T. S. Nunner, and P. J. Hirschfeld, Phys. Rev. B **74**, 060501(R) (2006).

[18] M. N. Gastiasoro and B. M. Andersen, Phys. Rev. B **98**, 184510 (2018).

[19] A. Ślebarski, M. Fijałkowski, P. Zajdel, M. M. Maśka, J. Deniszczyk, M. Zubko, O. Pavlosiuk, K. Sasmal, and M. B. Maple, Phys. Rev. B **102**, 054514 (2020).

[20] S. Miraglia, J. L. Hodeau, F. Bergevin, and M. Marezio, Acta Crystallogr. Sect. B **43**, 76 (1987).

[21] J. L. Hodeau, M. Marezio, and J. P. Remeika, Acta Crystallogr. Sect. B **40**, 26 (1984).

[22] https://www.aps.anl.gov/Beamlines/Directory.

[23] B. H. Toby and R. B. Von Dreele, J. Appl. Crystallogr. **46**, 544 (2013).

[24] J. Rodriguez-Carvajal, Physica B **192**, 55 (1993).

[25] I. G. Wood, K. S. Knight, G. D. Price, and J. A. Stuart, J. Appl. Crystallogr. **35**, 291 (2002); L. Vocadlo, K. S. Knight, G. D. Price, and I. G. Wood, Phys. Chem. Miner. **29**, 132 (2002).

[26] D. J. Singh and L. Nordstrom, *Planewaves, Pseudopotentials, and the LAPW Method*, 2nd ed. (Springer Science, New York, 2006).

[27] P. Blaha, K. Schwarz, G. K. H. Madsen, D. Kvasnicka, J. Luitz, R. Laskowski, F. Tran, and L. D. Marks, WIEN2k, *An Augmented Plane Wave + Local Orbitals Program for Calculating Crystal Properties* (Karlheinz Schwarz, Technische Universität Wien, Austria, 2001).

[28] A. Ślebarski, P. Zajdel, M. M. Maśka, J. Deniszczyk, and M. Fijałkowski, J. Alloys Compd. **819**, 152959 (2020).

[29] J. P. Perdew, A. Ruzsinszky, G. I. Csonka, O. A. Vydrov, G. E. Scuseria, L. A. Constantin, X. Zhou, and K. Burke, Phys. Rev. Lett. **100**, 136406 (2008).

[30] V. I. Anisimov, J. Zaanen, and O. K. Andersen, Phys. Rev. B **44**, 943 (1991).

[31] A. Wang, Z. Y. Nie, F. Du, G. M. Pang, N. Kase, J. Akimitsu, Y. Chen, M. J. Gutmann, D. T. Adroja, R. S. Perry, C. Cao, M. Smidman, and H. Q. Yuan, Phys. Rev. B **103**, 024503 (2021).

[32] I. W. H. Oswald, B. K. Rai, G. T. McCandless, E. Morosan, and J. Y. Chan, Cryst. Eng. Commun. **19**, 3381 (2017).

[33] A. Ślebarski, P. Zajdel, M. Fijałkowski, M. M. Maśka, P. Witas, J. Goraus, Y. Fang, D. C. Arnold, and M. B. Maple, New J. Phys. **20**, 103020 (2018).

[34] The Sn content is very similar for both samples (samples 1 and 2). However, the optimal stoichiometry to form the system requires a slight deficiency of Lu. Sample 2 meets these conditions, while in sample 1 we observed strong spatial Sn fluctuations, which are the reason for small tin alloy precipitates in areas where the compound of the 5-6-18-type shows a minimum of fluctuations roughly approximated by $\Lambda \sin(\frac{2\pi}{\Delta l} l)$, as shown in Fig. 1.

[35] Ch. Kittel, *Introduction to Solid State Physics*, 8th ed. (John Wiley and Sons, New York, 2004).

[36] Previously [37] we documented d-electron correlations with $U = 3$ eV for the similar $Ce_3Rh_4Sn_{13}$ and $La_3Rh_4Sn_{13}$ compounds and the impact of these correlations on the positive magnetoresistivity (MR) of these alloys. Similar positive MR effect is observed for $Lu_{5-\delta}Rh_6Sn_{18}$ sample 1 (see Fig. 13).

[37] A. Ślebarski, J. Goraus, P. Witas, L. Kalinowski, and M. Fijałkowski, Phys. Rev. B **91**, 035101 (2015).

[38] A. Ślebarski, J. Goraus, and P. Witas, Phys. Rev. B **92**, 155136 (2015).

[39] M. Gamża, W. Schnelle, A. Ślebarski, U. Burkhardt, R. Gumeniuk, and H. Rosner, J. Phys.: Condens. Matter **20**, 395208 (2008).

[40] S. M. Young, S. Zaheer, J. C. Y. Teo, C. L. Kane, E. J. Mele, and A. M. Rappe, Phys. Rev. Lett. **108**, 140405 (2012).

[41] N. F. Mott, *Metal-Insulator Transitions* (Taylor and Francis LTD, London, 1974).

[42] N. F. Mott, Philos. Mag. **13**, 989 (1966).

[43] First, we can exclude the contribution from tin as its H_c is below 0.1 T, and our materials are SC well above this value. Additionally, only one sample (sample 1) has Sn impurity, so the second one is free from this problem. Secondly, the bulk phase 5-6-18 and the disordered one have very similar T_c, hence it is difficult to separate the diamagnetic effect of the T_c bulk phase and $T_c^\star$ impurity one. Considering the similar T_c and $T_c^\star$ of the respective bulk and nanoscale disordered components of sample 1, one can only show the full Meissner effect observed below $T_c \approx T_c^\star$ (the case of sample 1 and 2).

[44] A. Mirmelstein, A. Junod, E. Walker, B. Revaz, J. Y. Genoud, and G. Triscone, J. Superconduct. **10**, 527 (1977).

[45] N. Kase, H. Hayamizu, and J. Akimitsu, Phys. Rev. B **83**, 184509 (2011).

[46] N. Kase, H. Hayamizu, K. Inoue, and J. Akimitsu, Physica C **471**, 711 (2011).

[47] K. Wang and C. Petrovic, Phys. Rev. B **86**, 024522 (2012).

[48] A. Bhattacharyya, D. T. Adroja, J. Quintanilla, A. D. Hillier, N. Kase, A. M. Strydom, and J. Akimitsu, Phys. Rev. B **91**, 060503(R) (2015).

[49] N. Kase, K. Inoue, H. Hayamizu, and J. Akimitsu, J. Phys. Soc. Jpn. **80**, SA112 (2011).

[50] A. Bhattacharyya, D. T. Adroja, N. Kase, A. D. Hillier, A. M. Strydom, and J. Akimitsu, Phys. Rev. B **98**, 024511 (2018).

[51] A. Ślebarski, J. Goraus, J. Deniszczyk, and Ł. Skoczeń, J. Phys.: Condens. Matter **18**, 10319 (2006).

[52] F. G. Aliev, N. B. Brandt, V. V. Moshchalkov, V. V. Kozyrkov, R. V. Skolozdra, and A. I. Belogorokhov, Z. Phys. B **75**, 167 (1989).

[53] A. Ślebarski, A. Jezierski, A. Zygmunt, S. Mähl, and M. Neumann, Phys. Rev. B **57**, 9544 (1998).

[54] A. Ślebarski, A. Jezierski, S. Lütkehoff, and M. Neumann, Phys. Rev. B **57**, 6408 (1998).

[55] P. Skornia, J. Goraus, M. Fijałkowski, and A. Ślebarski, J. Alloys Compd. **767**, 512 (2018).

[56] J. Spałek, A. Ślebarski, J. Goraus, L. Spałek, K. Tomala, A. Zarzycki, and A. Hackemer, Phys. Rev. B **72**, 155112 (2005).

[57] E. D. Bauer, A. Ślebarski, E. J. Freeman, C. Sirvent, and M. B. Maple, J. Phys.: Condens. Matter **13**, 4495 (2001).

[58] Z. Zhang, Y. Xu, C. N. Kuo, X. C. Hong, M. X. Wang, P. L. Cai, J. K. Dong, C. S. Lue, and S. Y. Li, Supercond. Sci. Technol. **28**, 105008 (2015).

[59] A. M. Strydom, J. Phys.: Condens. Matter **19**, 386205 (2007).

[60] T. P. Orlando, E. J. McNiff, Jr., S. Foner, and M. R. Beasley, Phys. Rev. B **19**, 4545 (1979).

[61] E. Helfand and N. R. Werthamer, Phys. Rev. Lett. **13**, 686 (1964); N. R. Werthamer, E. Helfand, and P. C. Hohenberg, Phys. Rev. **147**, 295 (1966).

[62] The carrier concentration n in $Lu_{5-\delta}Rh_6Sn_{18}$ is a few orders of magnitude smaller than the typical values for metals [63]. Thus, weaker screening of charged impurities can lead to fluctuations of the local chemical potential and induce spatial fluctuations of the superconducting order parameter Δ [64]. As a result, a transition to the superconducting state can be broad, as shown in Fig. 9. Previously, we found that in the case of disordered quasiskutterudites a simple Gaussian gap distribution $f(\Delta) \propto \exp[-\frac{(\Delta-\Delta_0)^2}{2D}]$ approximates the specific heat $C(T)$ and $\chi_{ac}(T)$ data in the vicinity of T_c [15], where Δ_0 and variance D of the distribution are treated as fitting parameters.

[63] V. Palenskis, World J. Conden. Matter Phys. **3**, 73 (2013).

[64] M. Ma and P. A. Lee, Phys. Rev. B **32**, 5658 (1985).

[65] E. Helfand and N. R. Werthamer, Phys. Rev. **147**, 288 (1966).

[66] P. G. de Gennes, Phys. kondens. Materie. **3**, 79 (1964); K. Maki, Physics **1**, 27 (1964); P. G. DeGennes, *Superconductivity in Metals and Alloys* (Benjamin, New York, 1966).

[67] In the approximation of $\frac{2\pi}{\Delta l} \rightarrow 0$ the fluctuations in composition of the sample disappear.

[68] P. E. Seiden, Phys. Rev. **179**, 458 (1969).

[69] P. Morel and P. W. Anderson, Phys. Rev. **125**, 1263 (1962).

[70] W. L. McMillan, Phys. Rev. **167**, 331 (1968).

[71] J. J. Hopfield, Phys. Rev. **186**, 443 (1969).

[72] E. S. Caixeiro, J. L. González, and E. V. L. de Mello, Phys. Rev. B **69**, 024521 (2004).

[73] A. Gurevich, Phys. Rev. B **67**, 184515 (2003).

[74] A. Ślebarski, J. Goraus, M. M. Maśka, P. Witas, M. Fijałkowski, C. T. Wolowiec, Y. Fang, and M. B. Maple, Phys. Rev. B **93**, 245126 (2016).

[75] A. Ślebarski and M. M. Maśka, Materials **13**, 5830 (2020).

[76] A. Ślebarski, M. M. Maśka, M. Fijałkowski, C. A. McElroy, and M. B. Maple, J. Alloys Compd. **646**, 866 (2015).

[77] M.-A. Méasson, D. Braithwaite, B. Salce, J. Flouquet, G. Lapertot, H. Sugawara, H. Sato, and Y. Onuki, J. Magn. Magn. Mater. **310**, 626 (2007).